AN ABSTRACT OF THE RESEARCH PROJECT REPORT

Paria Ghorbani for the degree of Master of Science in Geophysics presented on September 20, 2016.

Title: Earthquake Relocation in Three-Dimensional Velocity Models for Central Cascadia Continental Margin

Abstract approved:

_____

We used data from Cascadia Initiative and Blanco Transform Fault Zone array of ocean bottom seismometers and hydrophone to look at the seismicity and specially depth of the Central Cascadia Continental Margin events. Events were detected and located automatically with Antelope software package (Boulder Real Time Technologies). We looked at the seismicity in a 1-degree square region (44N-45N and 124W-125W) of the Cascadia Subduction Zone from 2012 to 2013. There were about 40 events in our catalog which was more than any other land network catalogs as we expected. Automatic earthquake location procedure sometimes associated with respectively large residuals for sharp arrivals for stations in strongly heterogeneous structure that associated with continental margin and subduction zones. These large residuals force us to remove them from location procedure because they cannot be associated in a simple velocity model. For smaller events that even can remove the event from the catalog because of small number of sufficient arrival in close stations. We selected 7 larger events (with local magnitudes greater than 2) which were located by other networks before to preform accurate depth analysis. We used and 2.5D model based on the position along one of ORWELL Lines (Gerdom et al., 2000) that are closed to the area (44.75N). We located hypocenters in resulting 3D model in NonLinLoc (Lomax et al., 2000). We used a very fine grid spacing of 500 m, different distance weighting and phase inclusion/omission strategies to locating hypocenters in NonlinLoc. In order to reduce the azimuthal gap, we combined the OBS data with land station data. Our

earthquake relocation results in overall shift of 7 km to the west in seismicity pattern. Based on depth results 1 out of 7 events occurred in overriding plate. 5 events seem be occurred on plate interface and one event depth is located in the base of oceanic crust. Plate inter face in our model is located in about 15 km depth. In order to get better understanding of seismicity and including more reliable S arrivals in our analysis we have to adjust Vp/Vs ratio on continental block of the model and relocate all events on continental margin with grid-search methods that contains S arrival picks as well.

©Copyright by Paria Ghorbani
September 20, 2016
All Rights Reserved

Earthquake Relocation in Three-Dimensional Velocity Models for Central Cascadia Continental Margin

by
Paria Ghorbani

A RESEARCH PROJECT REPORT

submitted to

Oregon State University

in partial fulfillment of
the requirements for the
degree of

Master of Science

September 20, 2016
Commencement June 2017

Master of Science thesis of Paria Ghorbani presented on September 20, 2016

APPROVED:

Major Professor, representing Major Name

Head (Chair or Director) of the Department (School, College) of (department name)

Dean of the Graduate School

I understand that my thesis will become part of the permanent collection of Oregon State University libraries. My signature below authorizes release of my thesis to any reader upon request.

Paria Ghorbani

Student Name, Author

ACKNOWLEDGEMENTS

There many people that I need to thank them for providing helps and supports during my time in here for performing this project.

First I would like to thank John Nabelek who provided funding and great project for me. His guidance and helps on every steps of this project was extremely useful. John, the beginning of this project was an adventure in Melville that I will never forget that.

I also need to thank Jochen Braunmiller who was always available to guide me in different steps of project. Jochen, your supports either here in OSU or USF was very important to me. I also need to thank Anne Trehu for her scientific helps and comment, I would like to thank Gary Egbert for accepting to be in my committee and reviewing the manuscript.

I need to thank my two lab friends, Bridget Hass and Birat Sapkota. The first few years in Corvallis would have been so tough without your supports. Bridget, your supports after your graduation helped me extensively.

To my friend Sahar for her non-scientific helps. It would have been impossible to do this project without your supports.

Finally, thanks to my family here and in Iran. Sardar, you are always kindest and most supportive friend. Mom, dad, I can't explain by word in these few lines how helpful you were to me, although our physical distance was almost half the world and I was not able to visit you for more than two years. Thanks for everything, you were always in my heart and I love you.

CONTRIBUTION OF AUTHORS

John Nabelek and Jochen Braunmiller contributed on writing this manuscript by providing general scientific comments and edits. They also helped on editing and cleaning the figures. Anne Trehu contributed on performing this project by providing help on selecting best choice of Velocity model for the region of study.

TABLE OF CONTENTS

Page

1 Introduction 4

2 Data and Methods 6

2.1 Detecting and associating the events 6

2.2 Database cleaning procedure 7

2.3 Improving the velocity model: 7

2.4 Depth distribution of the earthquakes: 8

2.5 NonLinLoc Analysis: 8

2.5.1 Three-dimensional Probabilistic Earthquake Location method: 9

2.5.2 Grid spacing and assumptions about stations depth on grid 10

2.5.3 Distance Weighting and Arrival Picks selection 11

3 Discussion and Conclusion 30

3.1 Results and Discussion: 30

3.2 Conclusion: 31

References: 46

LIST OF FIGURES

Figure **Page**
Figure 2-1: Cascadia Initiative array in year1 12
Figure 2-2: Blanco Transform Fault Zone and Cascadia Initiative year2 arrays 13
Figure 2-3: Year1 seismicity after automatic detection and association 14
Figure 2-4: Year1 seismicity after manual picking review. 15
Figure 2-5: Travel-time curves for P and S arrivals. 16
Figure 2-6: Depth distribution of the events in Year1. 17
Figure 2-7: Catalog 's comparison 18
Figure 2-8: Cross-section of P wave 3D velocity model 19
Figure 2-9: Cross-section of S wave 3D velocity model 20
Figure 2-10: : Two possible cases for water layer and crust layer boundary 21
Figure 2-11: Station coverage for events in 2012. 22
Figure 2-12: Station coverage for events in 2013. 23
Figure 2-13: 27
Figure 2-14: 28
Figure 2-15: 29
Figure 3-1: Residuals for Event#1, Only P arrival used for location 32
Figure 3-2: Residuals for Event#1, Only P arrival used for location 33
Figure 3-3: Residuals for Event#3, Only P arrival used for location 34
Figure 3-4: Residuals for Event#4, Only P arrival used for location 35
Figure 3-5: Residuals for Event#5, Only P arrival used for location 36
Figure 3-6: Residuals for Event#6, Only P arrival used for location 37
Figure 3-7: Residuals for Event#7, Only P arrival used for location 38
Figure 3-8: Residuals based on azimuth and distance for Event#1 39
Figure 3-9: Residuals based on azimuth and distance for Event#2 40
Figure 3-10: Residuals based on azimuth and distance for Event#3 41
Figure 3-11: Residuals based on azimuth and distance for Event#4 42
Figure 3-12: Residuals based on azimuth and distance for Event#5 43
Figure 3-13: Residuals based on azimuth and distance for Event#6 44
Figure 3-14: Residuals based on azimuth and distance for Event#7 45

LIST OF TABLES

Table Page

Table 2-1: Tapering P arrivals' weight. method1 24
Table 2-2: Tapering P arrivals' weight. method2 24
Table 2-3: Relocation results using grid-search algorithm, using only P arrivals 25
Table 2-4: Relocation results using Grid-search algorithm, method1. 25
Table 2-5: Relocation results using Grid-search algorithm, method2. 26
Table 2-6: Relocation results with HYPO71 26

1 Introduction

The Cascadia Subduction Zone (CSZ) megathrust is a thrust fault that extends for about 1000 km from Northern Vancouver Island to Cape Mendocino California. CSZ separates the Gorda, Juan de Fuca and Explorer plates from the North American plate. New oceanic crust is created offshore along the Gorda, Juan de Fuca and Explorer ridges and the plates are moving toward and eventually subducting beneath the North American continental plate.

There are different types of slip behavior along this plate boundary ranging from great earthquakes to tremors and episodic slow slip events. Geological records such as coseismic subsidence of estuaries, tsunami inundation, and deep sea turbidites show that multiple great earthquakes have occurred on the CSZ (Goldfinger et al., 2012). There is estimation of 18 ruptures during last 9800 years with an average recurrence interval of 600 years and individual intervals ranging from 215 to 1488 years (Goldfinger et al., 2003) with the most recent great rupture occurring in 1700 (e.g., Satake et al., 1996, 2007).

At the CSZ Juan de Fuca plate subducts beneath the North American plate at about 4 cm/yr (e.g., McCaffrey et al., 2007) but the CSZ is notable among other subduction zone for being seismically anomalously quiet and its lack of small to moderate magnitude earthquakes on the plate boundary interface fault. The first moderate-sized events on the plate interface have been documented only recently offshore Oregon where a few of these events have been recorded on the CSZ in distinct clusters of earthquakes (Trehu et al., 2008, 2012, 2015; Williams et al., 2011). These events are thought to be low angle thrust events related to high fluid content due to metamorphic phase transitions in the subducting slab and the interaction between a subducting seamount and the Siletz terrane of the overriding plate (Trehu et al., 2008, 2012; Williams et al., 2011). From 1989 through 2014, 10 earthquakes were recorded with magnitude greater than 3 (Trehu et al. 2015).

All documented events on palate interface have locations based on 1D models us but Earthquake location with simple 1D model in strongly heterogeneous structure such as continental margin and subduction zones is associated with many assumptions about distance weighting or inclusion/omission of certain phases. Hypocenteral location is affected by many factors such as network geometry, phase picking accuracy and velocity model that we are using for locating earthquakes. Utilizing 3D velocity structure instead of 1D or 2D layered structure model can help us to reduce the errors in calculating travel times, reduce the number of mentioned assumptions and therefor getting better results in hypocenteral location.

Here, we used a 2.5D model based on the position along ORWELL Lines (Gerdom et al., 2000) that are closed to the area (44.75N) and generated 3D velocity grid for using in NonLinLoc package (Lomax et al., 2000).

2 Data and Methods

We used data from the Cascadia Initiative (CI; year1 and year2, Toomey et al., 2014) and Blanco Transform Fault Zone arrays of ocean bottom seismometers and hydrophones to investigate the seismicity of the Juan de Fuca and Gorda plate regions. The OBSs incorporate new trawl-resistant shields, which also aid in shielding from ocean-bottom currents to enable the deployment of sensors in marine sediments directly above Cascadia locked zone.

As part of the CI deployment in year1 (2011-2012), the CI array consisting of 70 stations was deployed across the northern Juan de Fuca plate, while in year2 (2012-2013) the array was redeployed in the Gorda plate region. Concurrently with the CI year2 deployment, an independent array of 55 instruments was deployed along the Blanco Transform Fault Zone (BTFZ) (Figures 2-1 and 2-2).

2.1 Detecting and associating the events

Detecting earthquakes from continuous waveforms can be accomplished by different methods including simple short-term average divided by long-term average (STA/LTA) amplitudes or more advanced methods like array-based waveform correlation or matched filter techniques (e.g., Morton and Bilek, 2015).

Here, automatic event detection and initial location were preformed using the Antelope Software Package (Boulder Real Time Technologies). We utilized Antelope's standard detector (dbdetect), association (dbgrassoc) and location program (dbgenloc). (Pavlis et al., 2004).

Dbdetect identifies potential event arrivals by calculating the (STA/LTA) ratios on channels specified by user and flags the times when specified detection parameters are satisfying as a

potential seismic arrival signal. Initially, we tested different parameters for detection to calibrate dbdetect to detect the smallest event possible while minimizing spurious event detection.

dbgrassoc searches for a group of arrivals which were flagged by dbgenloc before and satisfies association parameters. The association parameters may include minimum number of stations, cluster time window. dbgrassoc uses dbgenloc program with a specified 1D velocity model and travel time grid, iteratively, to find the hypocenter location.

We ran dbgrassoc with different parameters to calibrate dbgrassoc for our study region. We mainly tested different parameter values for (1) cluster time window (2) minimum number of stations required for association to be claimed as an event and (3) weighting functions based on distance from event for stations.

During year1 about 300 regional events were detected and only a few of them occurred within the array. The majority of the events occurred on the BTFZ and the Juan de Fuca Ridge. In year2, with a dense arrays deployed in the highly active regions, over 20,000 seismic were well recorded.

2.2 Database cleaning procedure

In order to complete the automated detection and association procedure and to provide more precise locations, we manually reviewed waveforms of year1. We refined initial P arrival picks on the vertical components or hydrophones and also added as many S arrival picks as possible from horizontal components at close stations to improve the depth estimation. Manual reviewing of the waveforms removed about 70 of the associated events due to poor quality of associated phases (Figures 2-3 and 2-4) leaving “233” events.

2.3 Improving the velocity model:

After manually reviewing the year1 database, resulting in 233 events, we obtained travel time curves for P and S waves (Figure 2-5). Fitted lines are showing the slowness of 14.659 (sec/°) for

P wave arrivals and 25.28 (sec/°) for S wave arrivals. Which means the P-wave velocity is 7.57 km/sec and the S-wave velocity is 4.39 km/sec.

2.4 Depth distribution of the earthquakes:

After manually reviewing the events and picking S waves on close stations we classified the events in 3 groups (Figure 2-6).

1) Events with depth < 10 km.
2) Events with 10 km < depth< 20 km.
3) Events with depth > 20 km.

We were interested in location and specially depth of earthquakes on Cascadia continental margin. In order to obtain a better estimate of event depth beneath the continental shelf (between 124° to 125° W) we decided to perform a more precise depth analysis by using NonLinLoc package, which is a probabilistic, Non-Linear, global-search Earthquake location program (Lomax et al., 2000).

2.5 NonLinLoc Analysis:

Many seismological studies are relying on the accuracy of earthquake location quality. Hypocenter location is affected by many factors such as network geometry, phase picking accuracy and velocity model that we are using for locating earthquakes. Utilizing 3D velocity structure instead of 1D or 2D layered structure model can help us to reduce the errors in calculating travel times.
To improve the location of events on the continental margin, we looked at the seismicity in a 1-degree square region (44N-45N and 124W-125W) from 2012 to 2013 (Figure 2-7). There were about 40 events in our catalog, which is, as expected, more than for any other network catalog. The automatic earthquake location procedure sometimes associated with respectively large residuals for sharp arrivals for stations in strongly heterogeneous structure that associated with continental margin and subduction zones. These large residuals force us to remove them from the location procedure because they cannot be associated in the simple velocity model that we used

for automatic event location. For smaller events that may even lead to removal of an event from the catalog because of an insufficient number of arrivals at close stations. We selected 7 larger events (with local magnitudes greater than 2), which were located by other networks before, to preform accurate depth analysis. We used a pseudo-3D model based on the position along the ORWELL lines (Gerdom et al., 2000) that are closed to the area (44.75° N) considered here. The pseudo-3D model generated by defining a set of polygons of different layers in the 2D cross-section of ORWELL line for different geological part of subduction zone and extending that cross section 40.44° to 48.49°N. We used a Vp/Vs ratio of 1.80 for crust and 1.85 for sediments to calculate S wave travel time grids.

This pseudo-3D grid is extended from Mendocino Triple Junction in southern side to Vancouver Island in northern side. The velocity grid extends from 122° to 131° W. Also the grid extends to 60 km depth (Figures 2-8 and 2-9). We located hypocenters in the resulting 3D model in NonLinLoc (Lomax et al., 2000).

2.5.1 Three-dimensional Probabilistic Earthquake Location method:

The probabilistic formulation of nonlinear inverse problems relies on the use of normalized and unnormalized probability density functions to express our knowledge about the values of parameters (Husen and Smith, 2004). If the probability density functions giving a priori information on the model parameters and on observations are independent, and the theoretical relationship relating a vector of observed data and unknown parameters can be expressed as a conditional density function, then a complete, probabilistic solution can be expressed as a posteriori probability density function (PDF) (Tarantola and Valette, 1982). In earthquake location, the unknown parameters are the hypocentral coordinates (x, y, and z) and the origin time T, the observed data are arrival times measured at seismograph stations, and the theoretical relation gives predicted or theoretical travel times. If the theoretical relationship and the observed travel times are assumed to have Gaussian uncertainties expressed by covariance matrices, and if the a priori information on the origin time is taken as uniform, the PDF can be evaluated analytically in

a marginal PDF for the spatial location and the origin time (Tarantola and Valette, 1982; Moser et al., 1992).

NonLinLoc has three different ways to calculate PDF (Lomax et al., 2000):

1) Via a grid-search algorithm using successively finer, nested grids which is the method that we chose our study. We used fine grid with 500 m spaced nodes.
2) Via a Metropolis-Gibbs sampling algorithm performing a directed random walk within a spatial volume to obtain a set of samples that follow the PDF
3) Via an Oct-Tree Importance sampling algorithm (Oct-Tree algorithm). The Oct-Tree algorithm gives accurate, efficient and complete mapping of the PDF of the earthquake location problem (Lomax and Curtis, 2001). It uses recursive subdivision and sampling of cells in three dimensions to generate a cascade of sampled cells, where the number of sampled cells follows the values of the PDF at the cell center, thus leading to higher density of cells in areas of higher PDF (lower misfit)

2.5.2 Grid spacing and assumptions about stations depth on grid

We used a fine grid with spacing of 500 mto generate velocity model and calculating travel times between each station in the grid and grid nodes.

In order to put the OBS stations elevation on ocean bottom in our grid we used below method:

In the first step we converted the station's longitude to the location on ORWELL line which were located on 44.75° N. We used SIMPLE transformation to convert station's geographical location to location the grid. SIMPLE transformation only corrects longitudinal distances as a function of latitude with below Algorithm:

x (on grid) = (long - longOrig) * 111.111 * cos(lat_radians);

y (on grid) = (lat - latOrig) * 111.111;

lat = latOrig + y / 111.111;

long = longOrig + x / (111.111 * cos(lat_radians));

longOrig and latOrig are corresponded to latitude and longitude of the grids origin. (131°W - 40.44°N for our grid)

After that we will find the two grid nodes in (in x direction) around the station location. Searching in generated velocity model, we can find the position of the nodes in water and crust (Figure 2-10). We shifted the location on point 4 in Figure 2-10 to force the OBS sensor be placed on oceanic crust layer. With 500 m grid node spacing the shift in station location is always less than 500 m.

2.5.3 Distance Weighting and Arrival Picks selection

For this study we used the grid-search algorithm around geographical location on clusters because it gives accurate and reliable mapping of the PDF in all grid nodes. In order to reduce the azimuthal gap, we combined the OBS data with land station data (Figures 2-11 and 2-12).

We utilized three different distance weighting strategy and arrival picks selection to locate hypocenters in NonLinLoc:

4) Grid-search algorithm, using only P arrivals with full weight to stations closer than 60 km and removing the arrivals from stations farther than 200 km (Tables 2-1 and 2-3, Figure 2-13).
5) Grid-search algorithm, using P arrivals with full weight to stations closer than 60 km and removing the arrivals from stations farther than 200 km combined with S arrivals using 50% weight for stations closer than 60 km (Tables 2-1 and 2-4, Figure 2-14).
6) Grid-search algorithm, using P arrivals with full weight to stations closer than 60 km and removing the arrivals from stations farther than 200 km combined with S arrivals using 50% weight for stations closer than 40 km (Tables 2-2 and 2-5 and Figure 2-15).

Trehu et al., (2015), located 5 out of 7 events in our using 1D velocity model (Same ORWELL line) and linearized HYPO71 (Lee and Lahr, 1972) method (Table 2-6). We compared our results with their locations in each part. Also we used their picks and weighting data for one of the evens in our catalog (Event# 3) three different strategies above (Figures 2-11, 2-12 and 2-13).

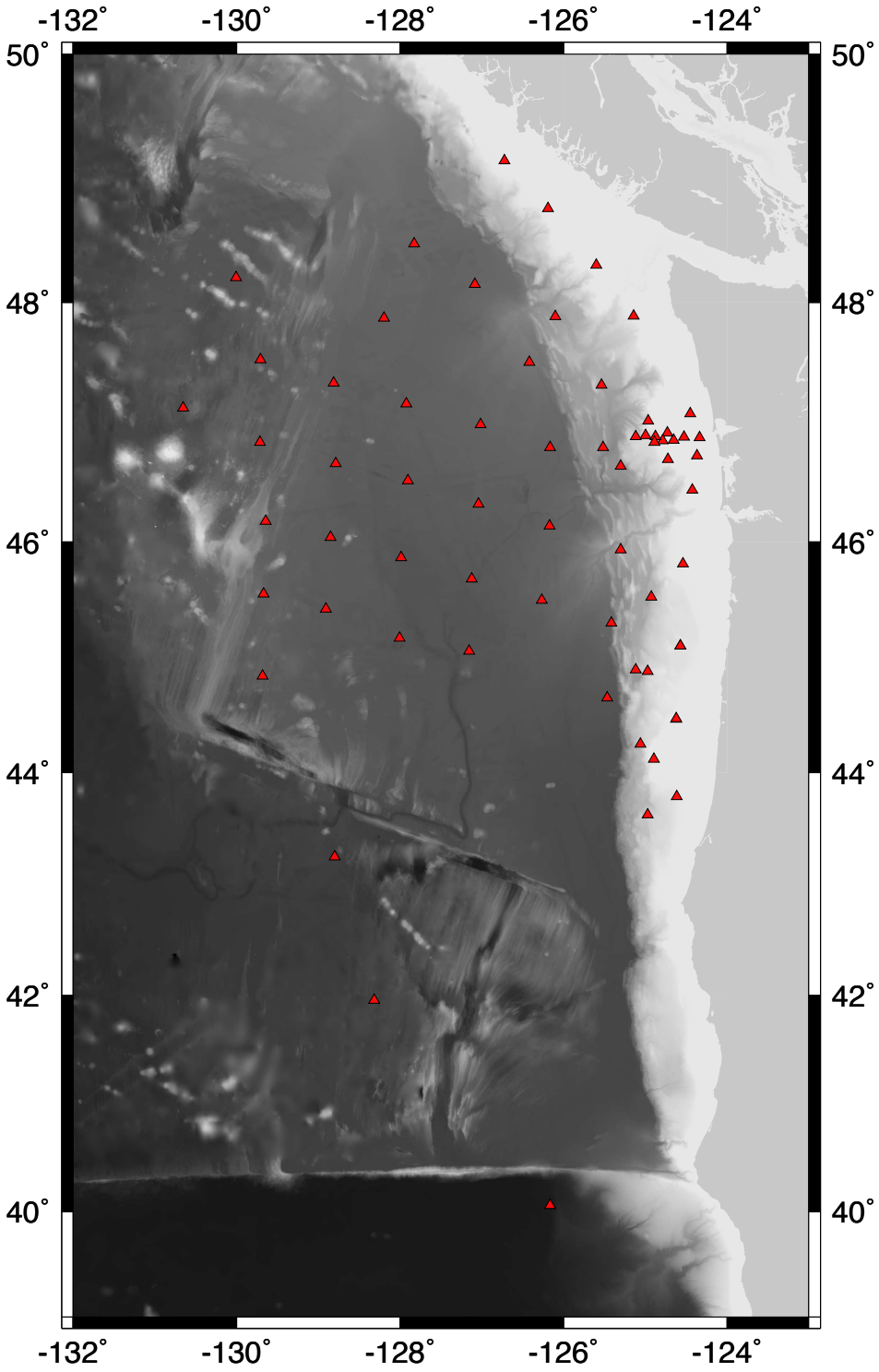

Figure 2-1: Cascadia Initiative array in year1

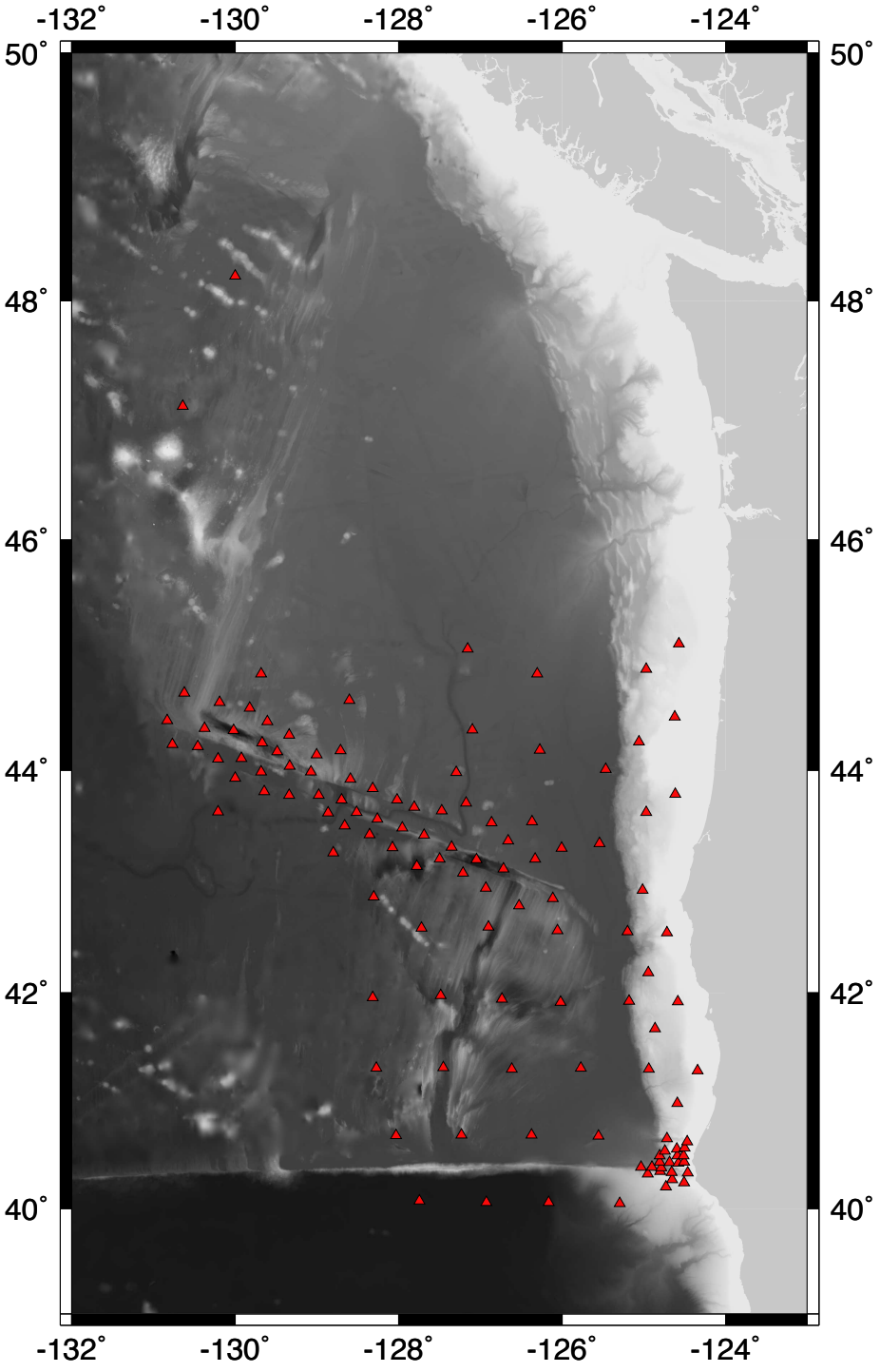

Figure 2-2: Blanco Transform Fault Zone and Cascadia Initiative year2 arrays

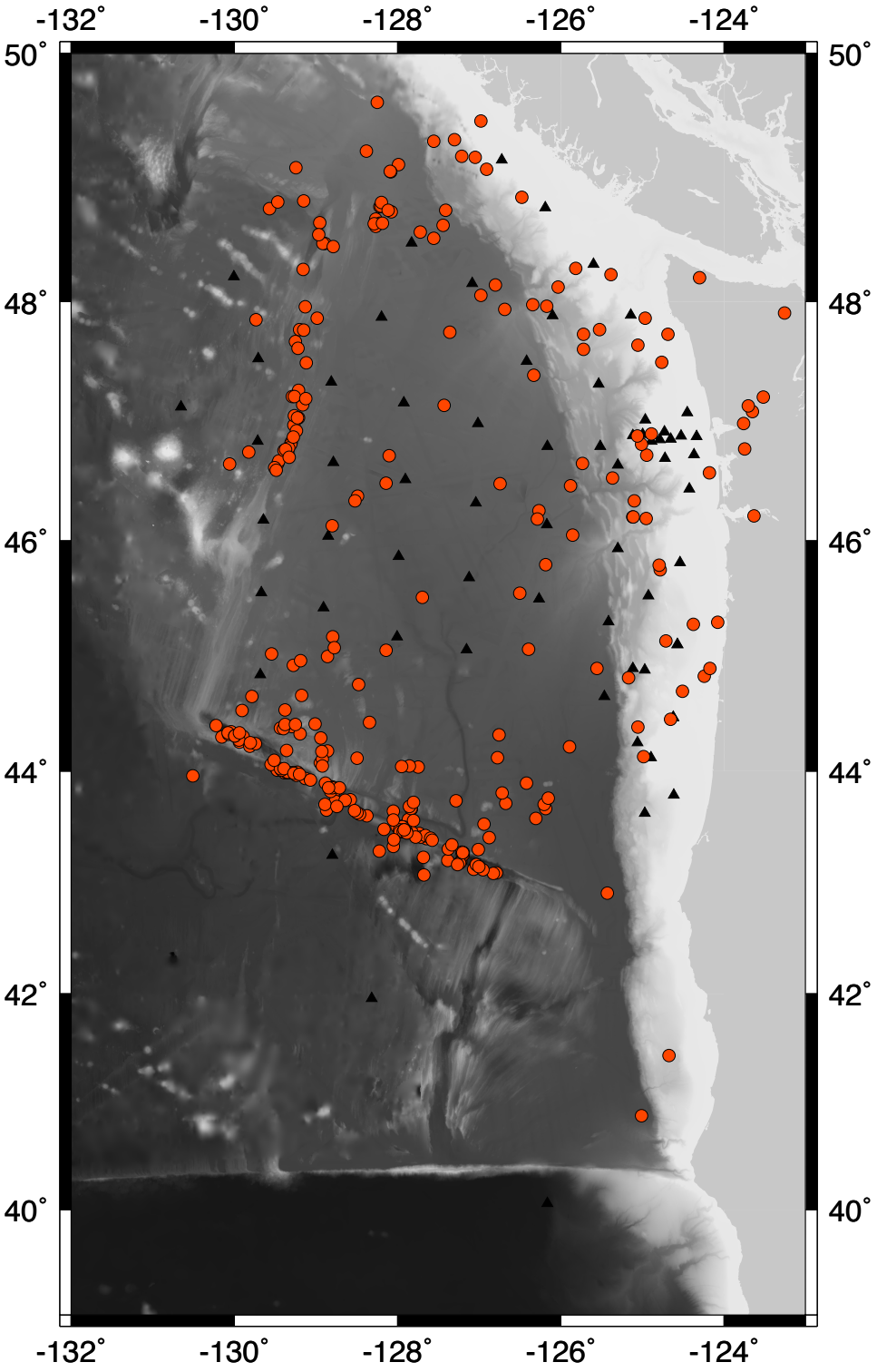

Figure 2-3: Year1 seismicity after automatic detection and association of the events. Total number of events is 304

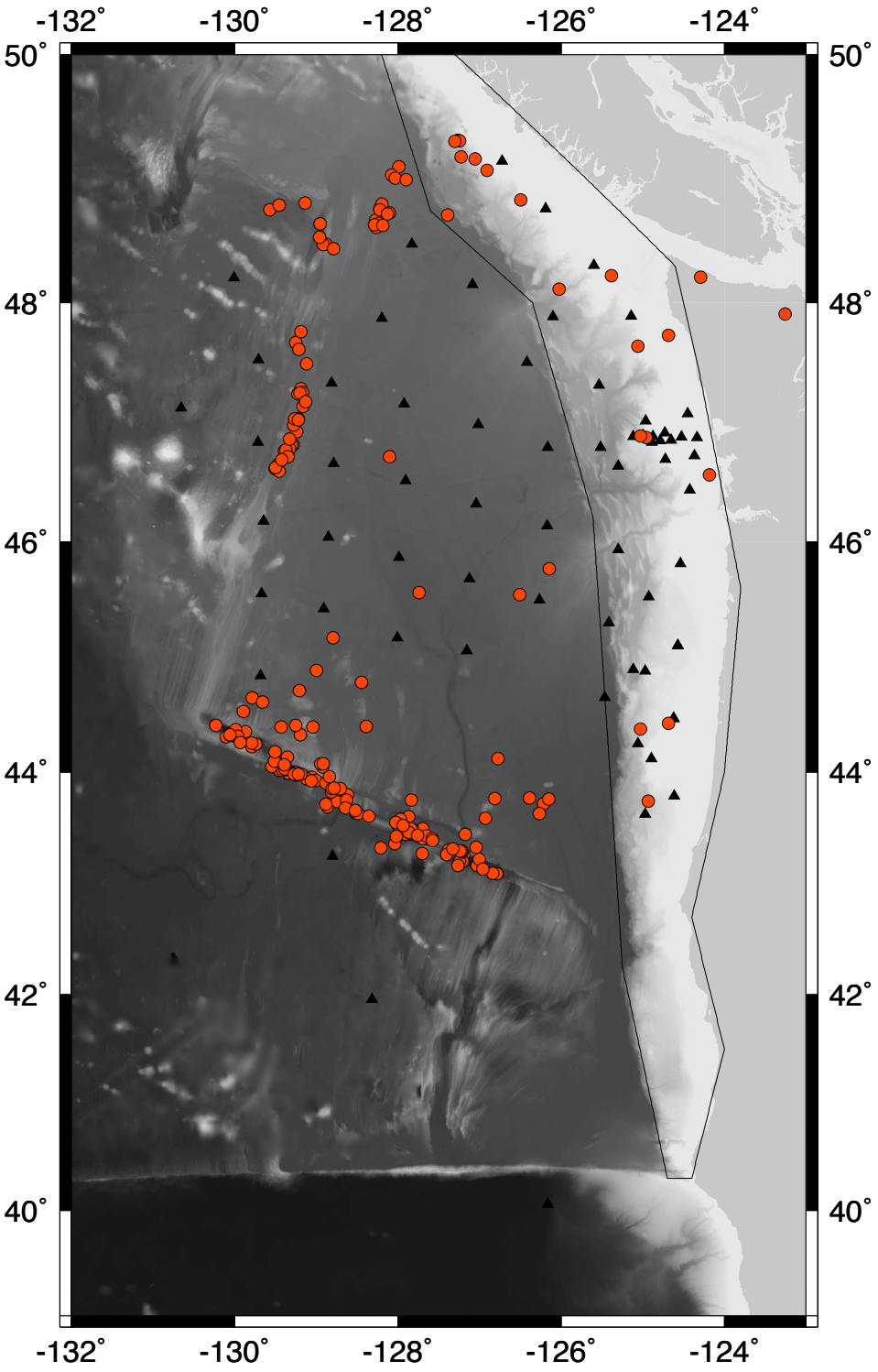

Figure 2-4: Year1 seismicity after manual picking review. Total number of events is 233.

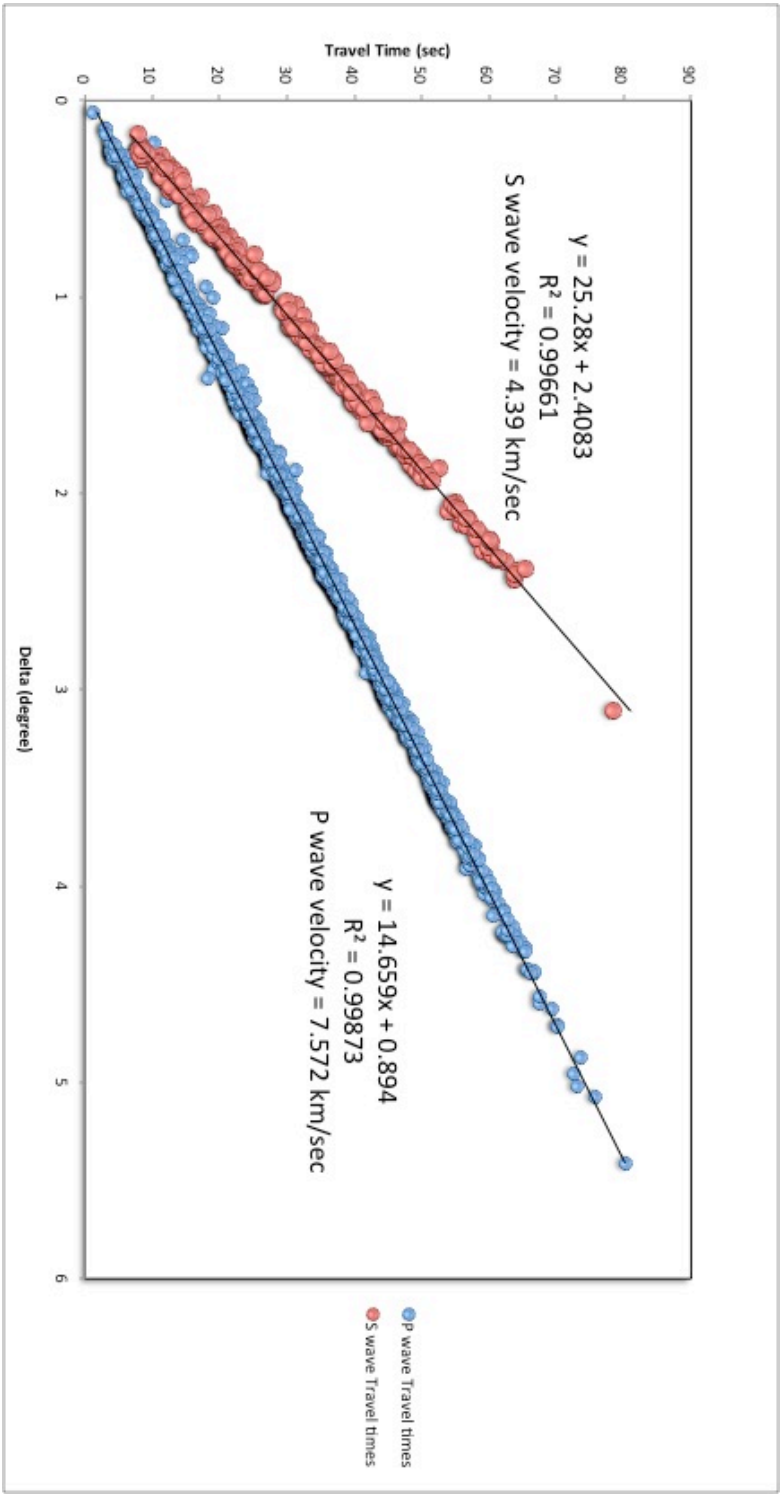

Figure 2-5: Travel-time curves for P and S arrivals. Blue and Red circles are showing the travel times for P and S waves. Fitted straight lines give average Pn wave velocity of 7.57 km/sec and Sn wave velocity of 4.39 km/sec.

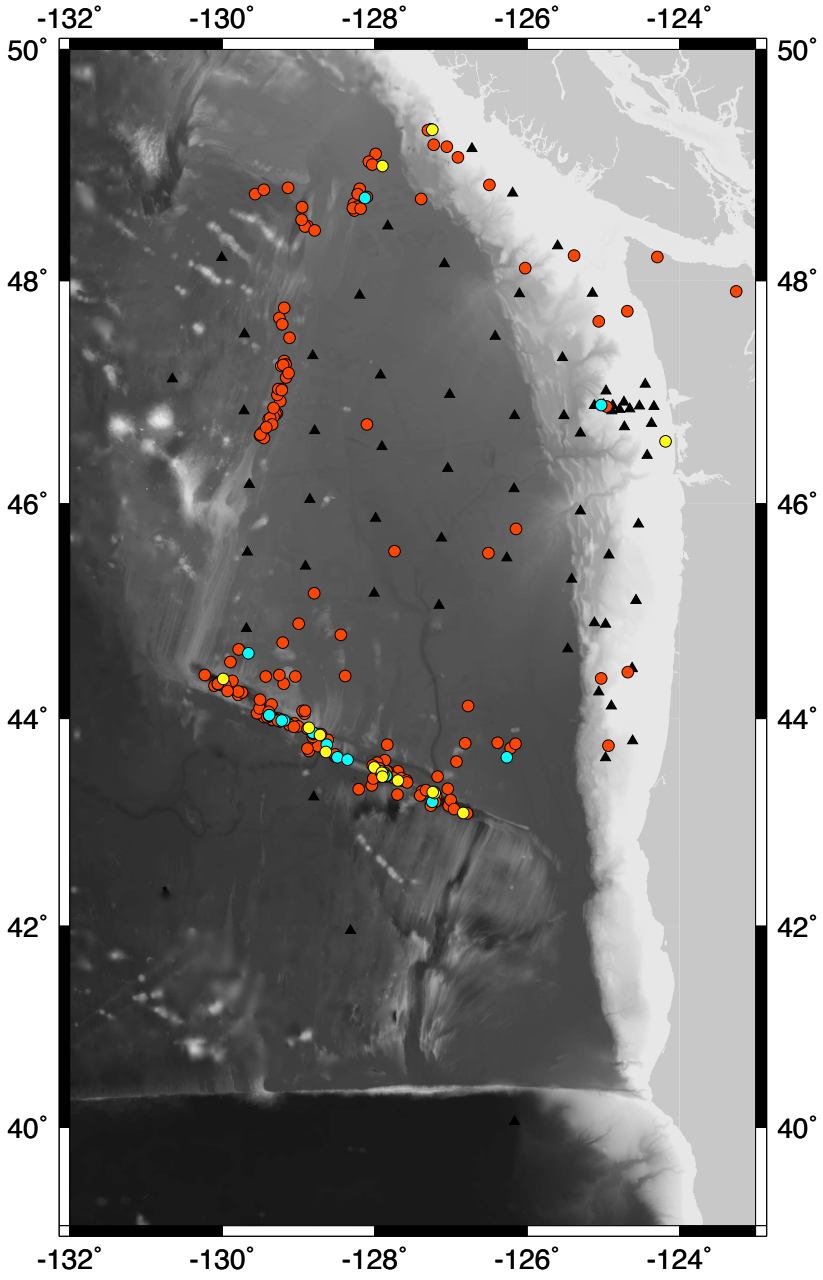

Figure 2-6: Depth distribution of the events in Year1. Orange circles events with depth < 10 km, turquoise 10 km < depth < 20 km, yellow depth > 20 km

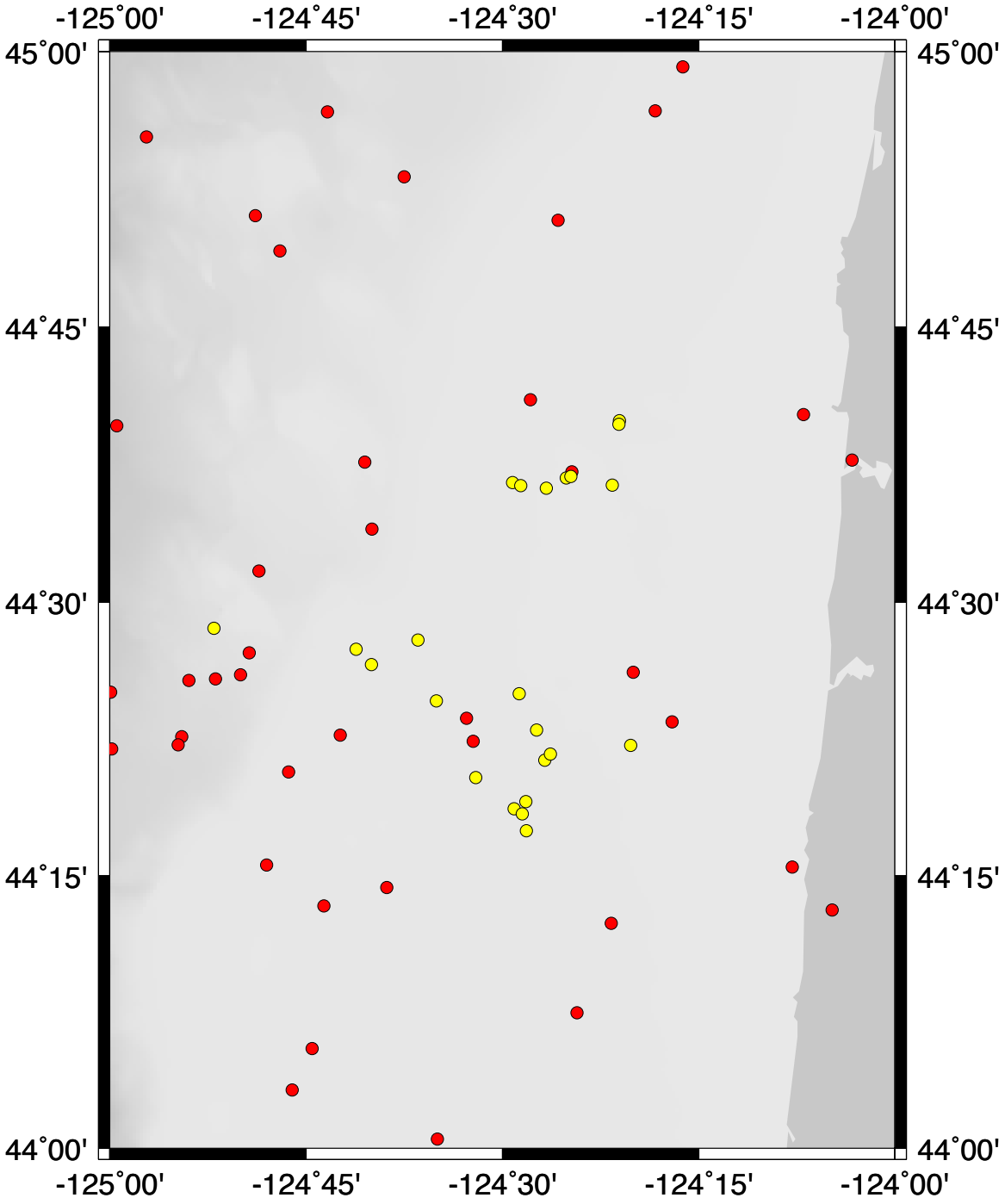

Figure 2-7: Red circles shows the epicenters with located by dbgenloc program using improved 1D velocity model in 2012 and 2013 time period. Total number of events is 40. Yellow circles are showing the events from Advanced National Seismic System (ANSS) Northern California Earthquake Data Center [NCEDC] catalog in the same time.

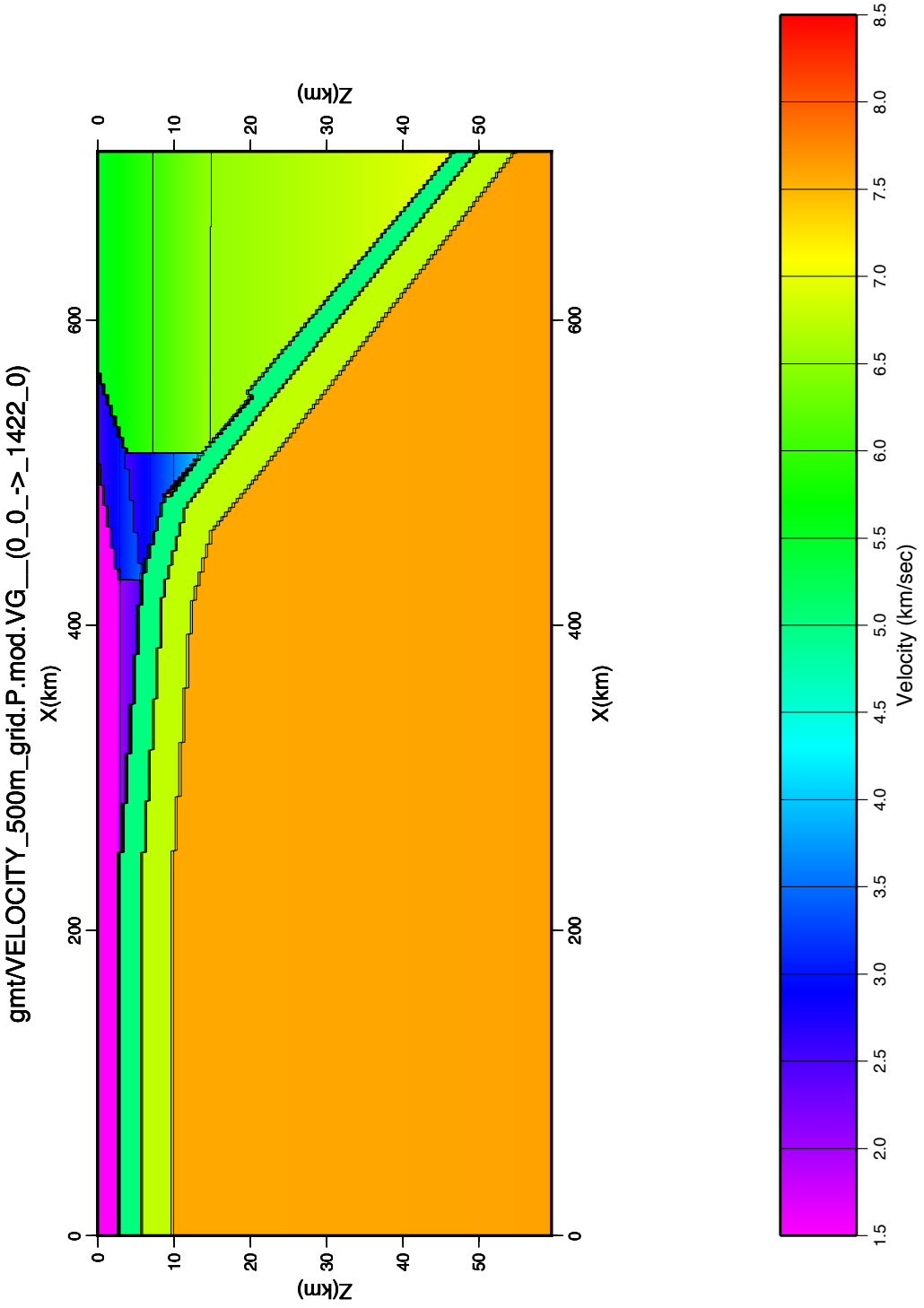

Figure 2-8: Cross-section of P wave 3D velocity model generated by Vel2Grid program (Lomax et al., 2004) based on ORWELL refraction line.

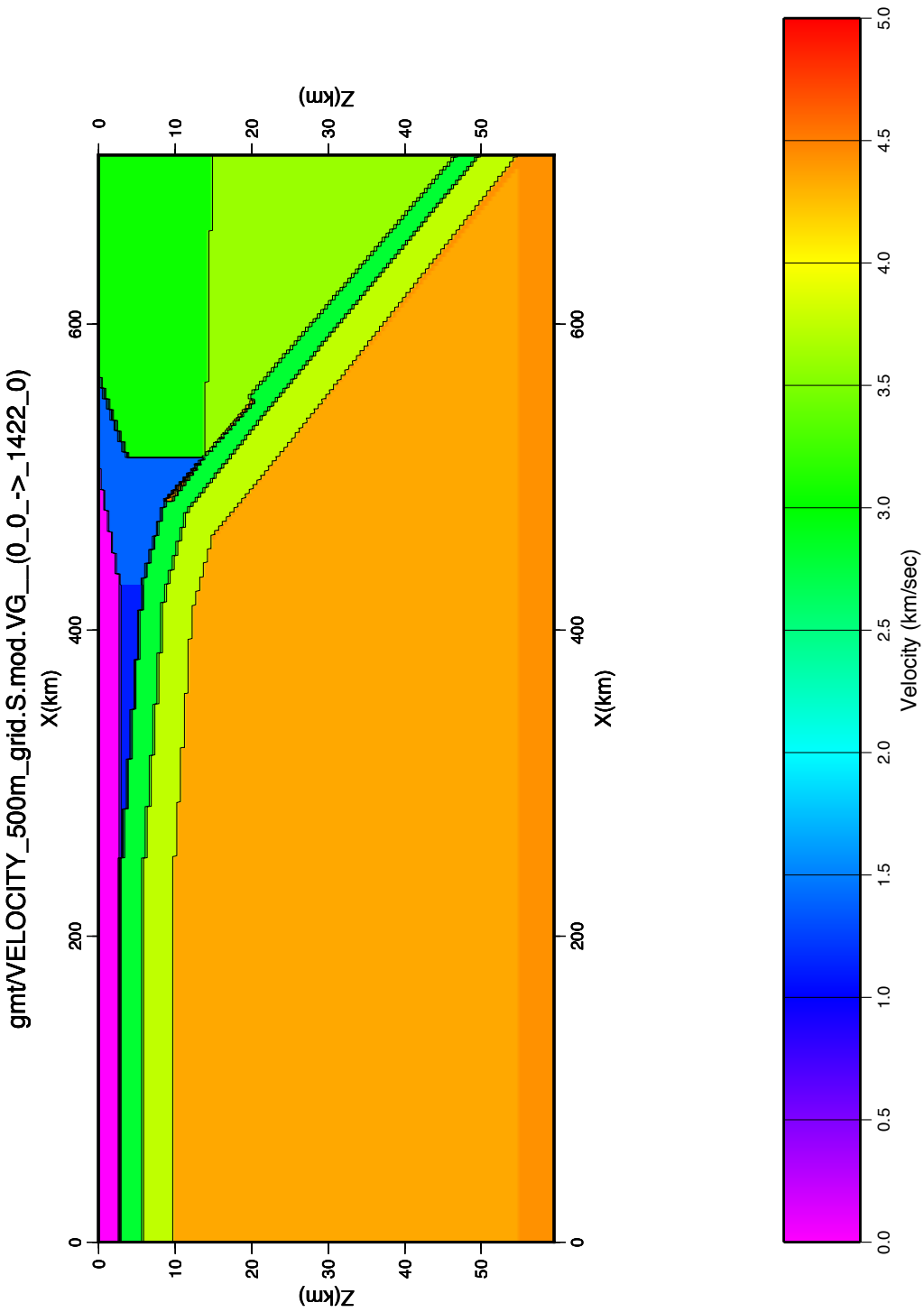

Figure 2-9: Cross-section of S wave 3D velocity model generated by Vel2Grid program (Lomax et al., 2004) based on ORWELL refraction line.

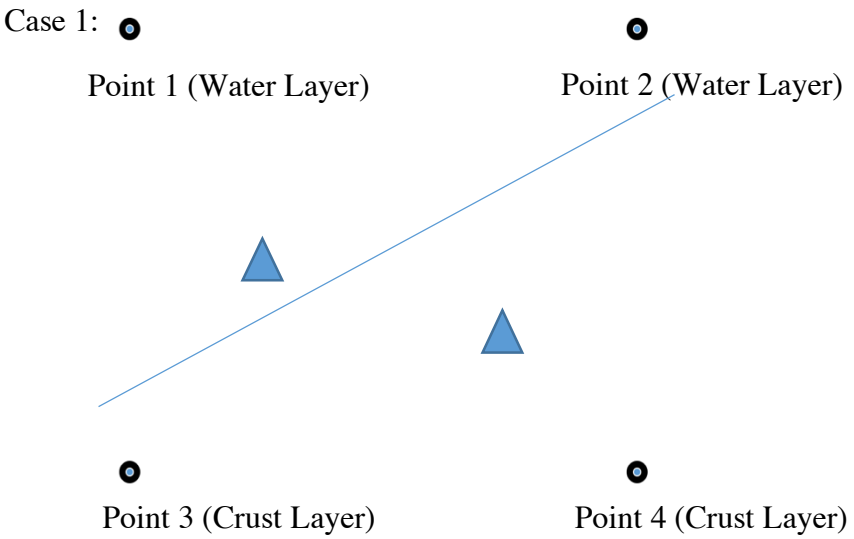

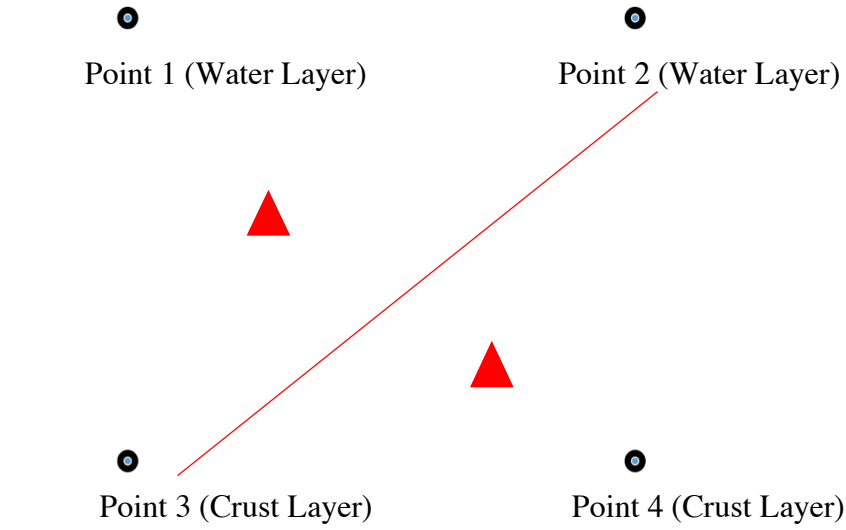

Figure 2-10: Two possible cases for water layer and crust layer boundary and 4 possible station's position between the grid nodes the grid nodes. In all cases Point4 is always inside the crust and shift in station's position is less than 500 m in X and Y directions.

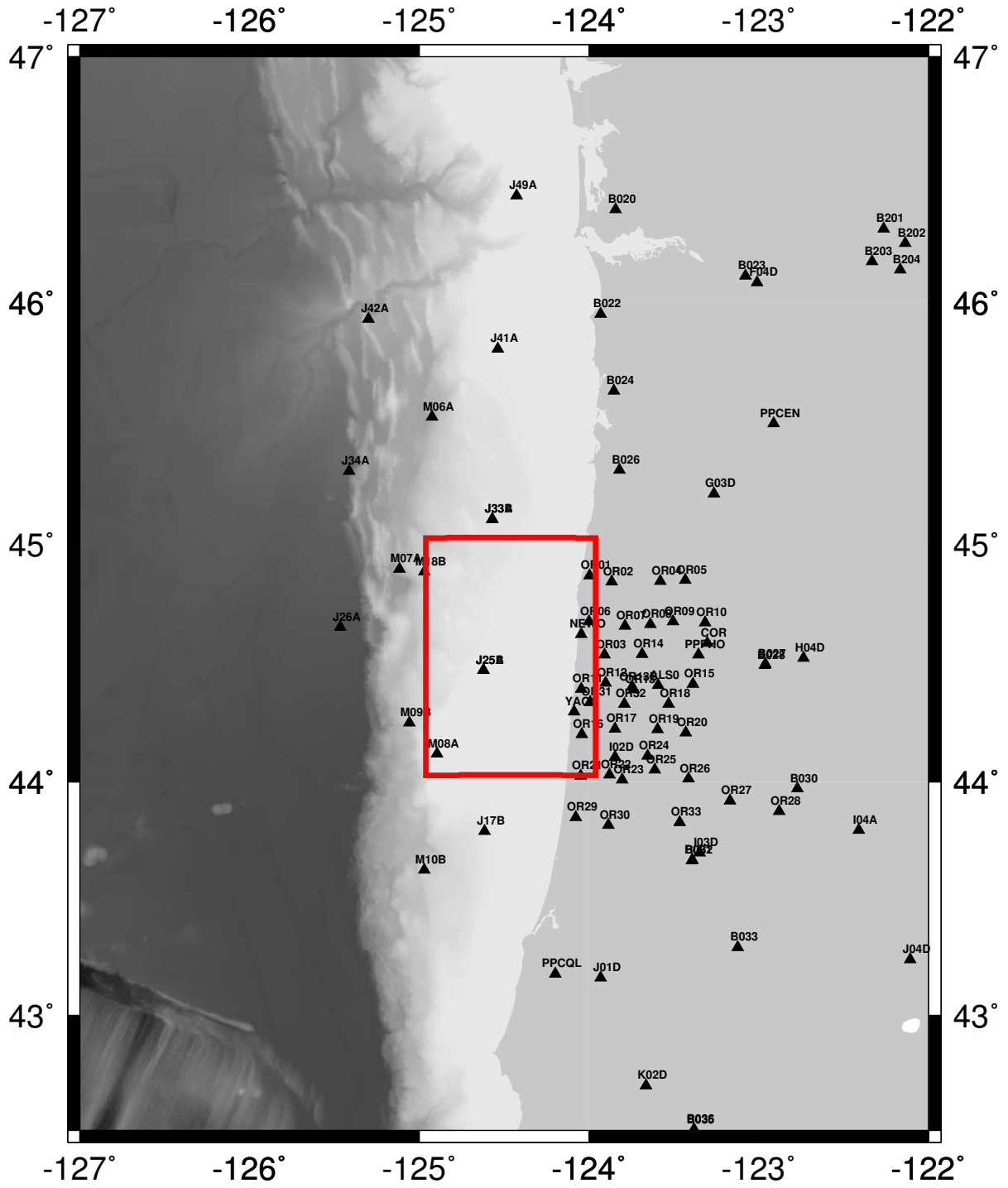

Figure 2-11: Station coverage for events in 2012. Red rectangle shows study area.

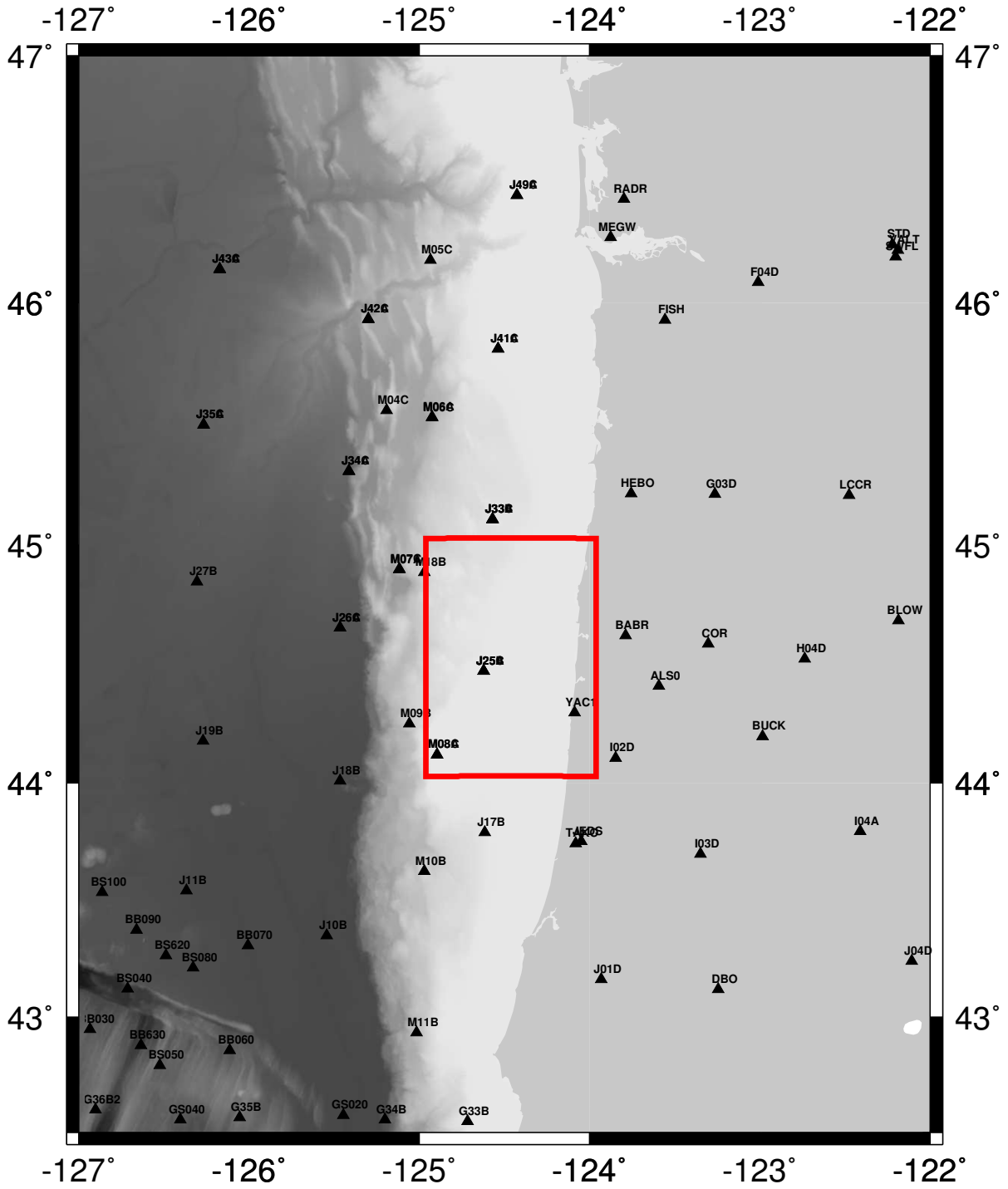

Figure 2-12: Station coverage for events in 2013. Red rectangle shows study area.

Distance (d)	Weight
d < 60 km	100 %
60 km < d < 120 km	75%
120 km < d < 160 km	50%
160 km < d < 200 km	25%
d > 200 km	0%

Table 2-1: Tapering P arrivals' weight. method1

Distance (d)	Weight
d < 40 km	100 %
40 km < d < 80 km	75%
80 km < d < 130 km	50%
130 km < d < 180 km	25%
d > 180 km	0%

Table 2-2: Tapering P arrivals' weight. method2

Event#	Date (YYYYmmdd)	Time (hhmm)	Origin (s)	Latitude (°)	Longitude (°)	Number of Picks	Azimuth GAP	Closest Station	rms (d)	Depth (km)
1	20120320	0843	46.92	44.3757	-124.506	23	85	14.74	0.47	9
2	20120320	0928	37.2	44.3847	-124.511	21	67	13.66	0.54	11
3	20120418	1521	0.22	44.6052	-124.379	25	71	23.26	0.31	18
4	20130125	0041	12.46	44.4252	-124.652	20	75	36.53	0.45	29.5
5	20130125	0343	7.99	44.4612	-124.635	18	72	1.5	0.53	15
6	20130125	0427	43.29	44.4432	-124.637	19	73	38.45	0.45	19.5
7	20130125	0858	33.15	44.3667	-124.62	20	77	11.66	0.57	6.5

Table 2-3: Relocation results using grid-search algorithm, using only P arrivals with full weight to stations closer than 60 km and removing the arrivals from stations farther than 200 km.

Event#	Date (YYYYmmdd)	Time (hhmm)	Origin (s)	Latitude (°)	Longitude (°)	Number of Picks	Azimuth GAP	Closest Station	rms (d)	Depth (km)
1	20120320	00843	46.9268	44.3757	-124.506	27	85.06	14.74	0.49	9.5
2	20120320	0928	37.1896	44.3847	-124.511	25	67.31	13.67	0.58	11.5
3	20120418	1521	0.244328	44.6007	-124.38	28	72.04	22.95	0.34	17.5
4	20130125	0041	12.4574	44.4297	-124.651	23	74.42	36.81	0.47	29.5
5	20130125	0343	7.97233	44.4657	-124.635	20	72.11	1.16	0.58	15
6	20130125	0427	43.3022	44.4522	-124.655	22	73.09	37.82	0.48	29.5
7	20130125	0858	33.1395	44.3712	-124.62	24	77.67	11.17	0.64	6.5

Table 2-4: Relocation results using Grid-search algorithm, using P arrivals with full weight to stations closer than 60 km and removing the arrivals from stations farther than 200 km combined with S arrivals using 50% weight for stations closer than 60 km or method1 in this study.

Event#	Date (YYYYmmdd)	Time (hhmm)	Origin (s)	Latitude (°)	Longitude (°)	Number of Picks	Azimuth GAP	Closest Station	rms (d)	Depth (km)
1	20120320	0843	46.9352	44.3937	-124.504	25	87.9675	13.3406	0.496314	11.5
2	20120320	0928	37.3297	44.4072	-124.515	24	68.6331	11.609	0.463181	12.5
3	20120418	1521	0.224068	44.6097	-124.379	25	70.7402	23.5796	0.305392	17.5
4	20130125	0041	12.3284	44.4702	-124.647	19	72.994	39.4348	0.418749	29.5
5	20130125	0343	8.17375	44.4297	-124.613	19	73.7155	4.73357	0.50832	11
6	20130125	0427	43.2621	44.4387	-124.625	16	73.3822	39.0315	0.388017	15.5
7	20130125	0858	32.9135	44.3622	-124.608	20	78.0426	12.2895	0.633531	5.5

Table 2-5: Relocation results using Grid-search algorithm, using P arrivals with full weight to stations closer than 60 km and removing the arrivals from stations farther than 200 km combined with S arrivals using 50% weight for stations closer than 40 km or method2 in this study.

Date (YYYYmmdd)	Time (hhmm)	Origin (s)	Latitude (°)	Longitude (°)	Number of Picks	Azimuth GAP	Closest Station	rms (d)	Depth (km)
20120418	1521	0.35	44.584	-124.29	21	70	19.8	0.33	18.3
20130125	0041	12.81	44.438	-124.554	16	91	6.6	0.36	14.4
20130125	0343	8.72	44.429	-124.573	14	92	6	0.23	14.4
20130125	0427	42.91	44.416	-124.55	11	115	4.6	0.32	16.7
20130125	0858	34.55	44.423	-124.552	14	93	7.8	0.31	13.7

Table 2-6: Relocation results with HYPO71 (LEE AND LAHR, 1972) analysis. Velocity model ORWELL3 and a Vp/Vs ratio of 1.85 were used for the 25 January 2013 earthquakes; ORWELL1 and Vp/Vs ratio of 1.77 were used for the 18 April 2012 event (Trehu et al., 2015)

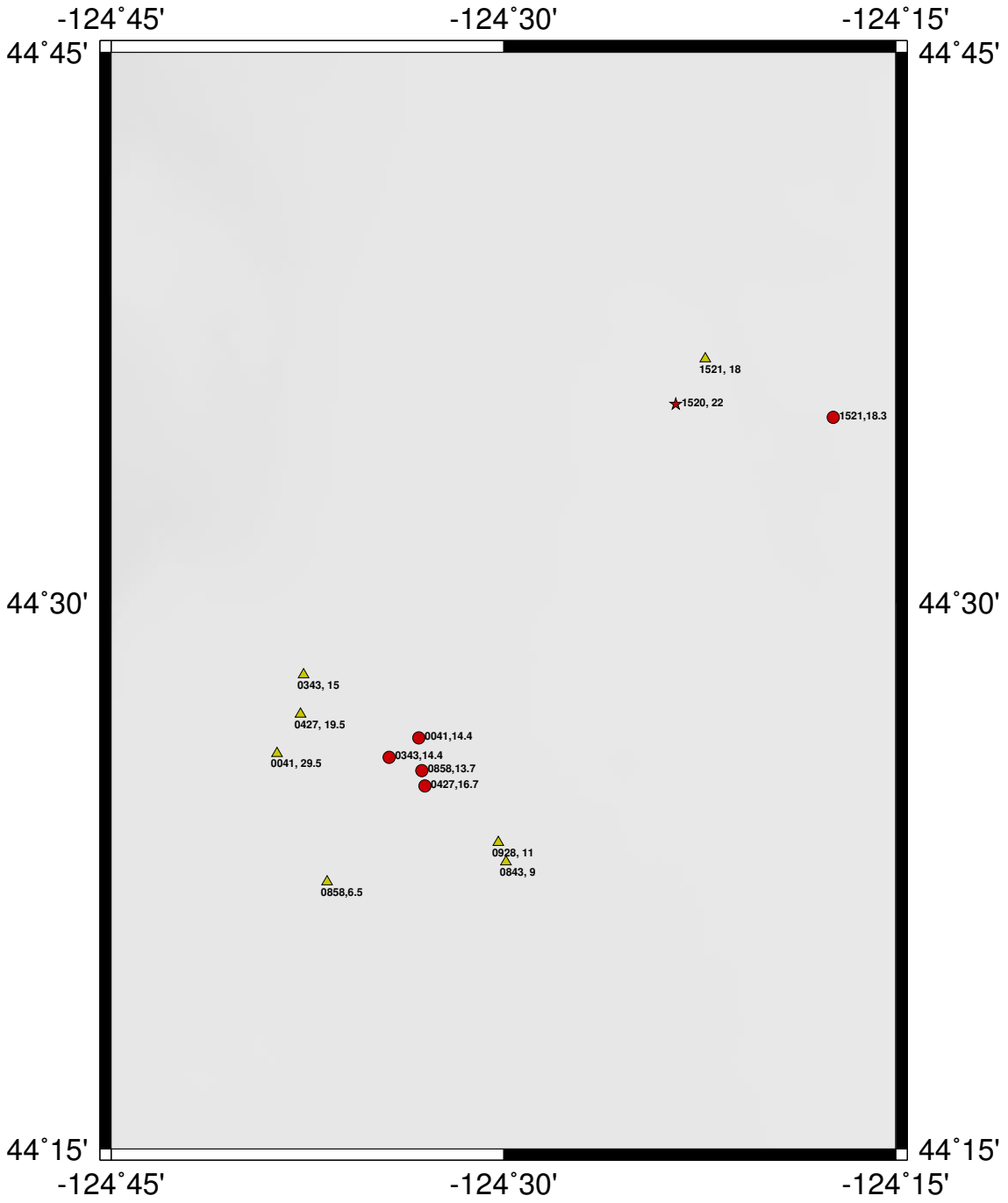

Figure 2-13: Yellow triangles shows the result of grid-search algorithm, using only P arrivals with full weight to stations closer than 60 km and removing the arrivals from stations farther than 200 km. Red circles are events that located with 1D model and HYPO71 (LEE AND LAHR, 1972) algorithm (Trehu et al., 2015). Red star shows the 18 April 2012 event with picks used by Trehu et al., 2015 and recent grid-search method. Labels are showing Origin Time and depth of the events.

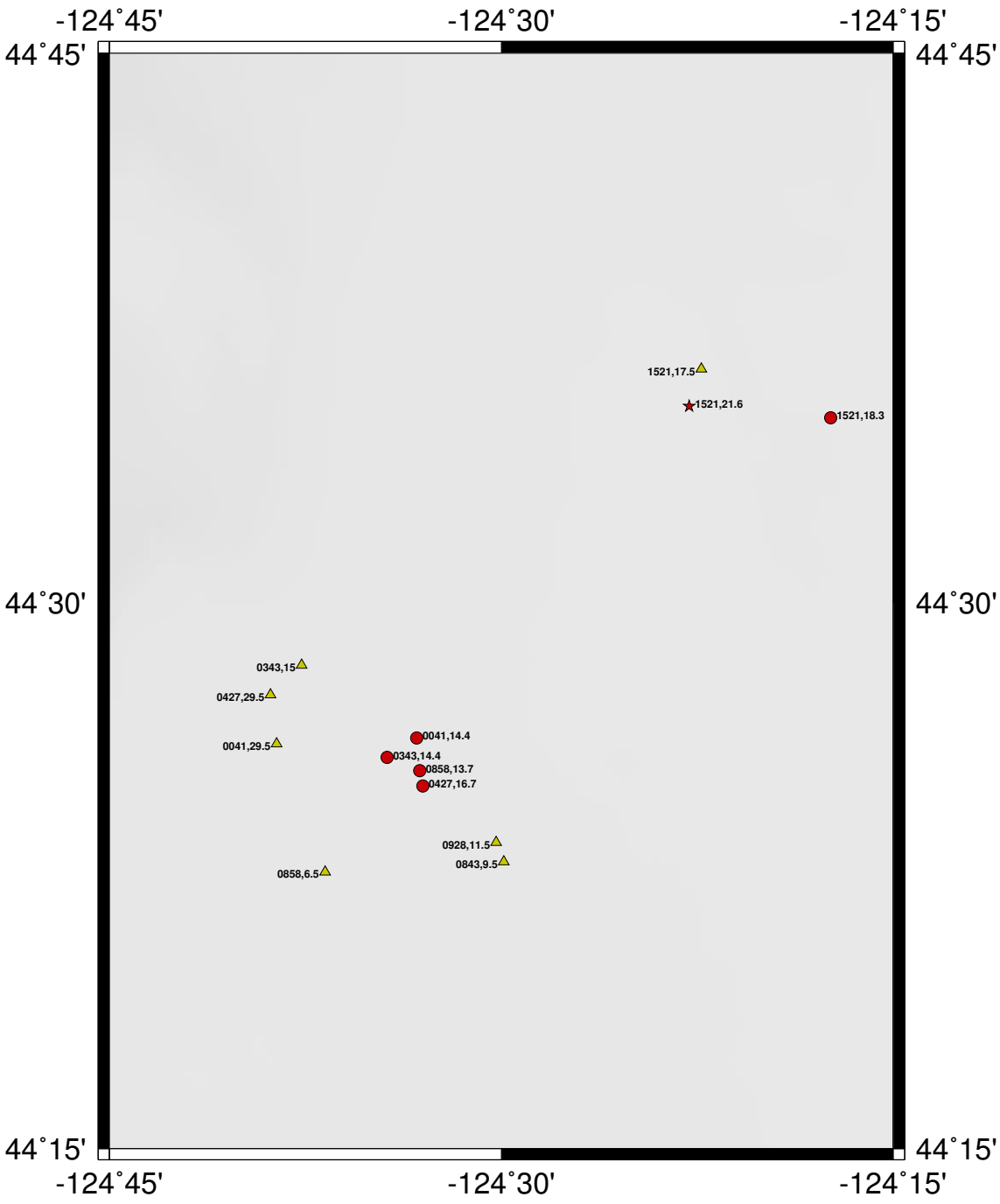

Figure 2-14: Yellow triangles shows the result of grid-search algorithm, using P arrivals with full weight to stations closer than 60 km and removing the arrivals from stations farther than 200 km combined with S arrivals using 50% weight for stations closer than 60 km. Red circles are events that located with 1D model and HYPO71 (LEE AND LAHR, 1972) algorithm (Trehu et al., 2015). Red star shows the 18 April 2012 event with picks used by Trehu et al., 2015 and recent grid-search method. Labels are showing Origin Time and depth of the events.

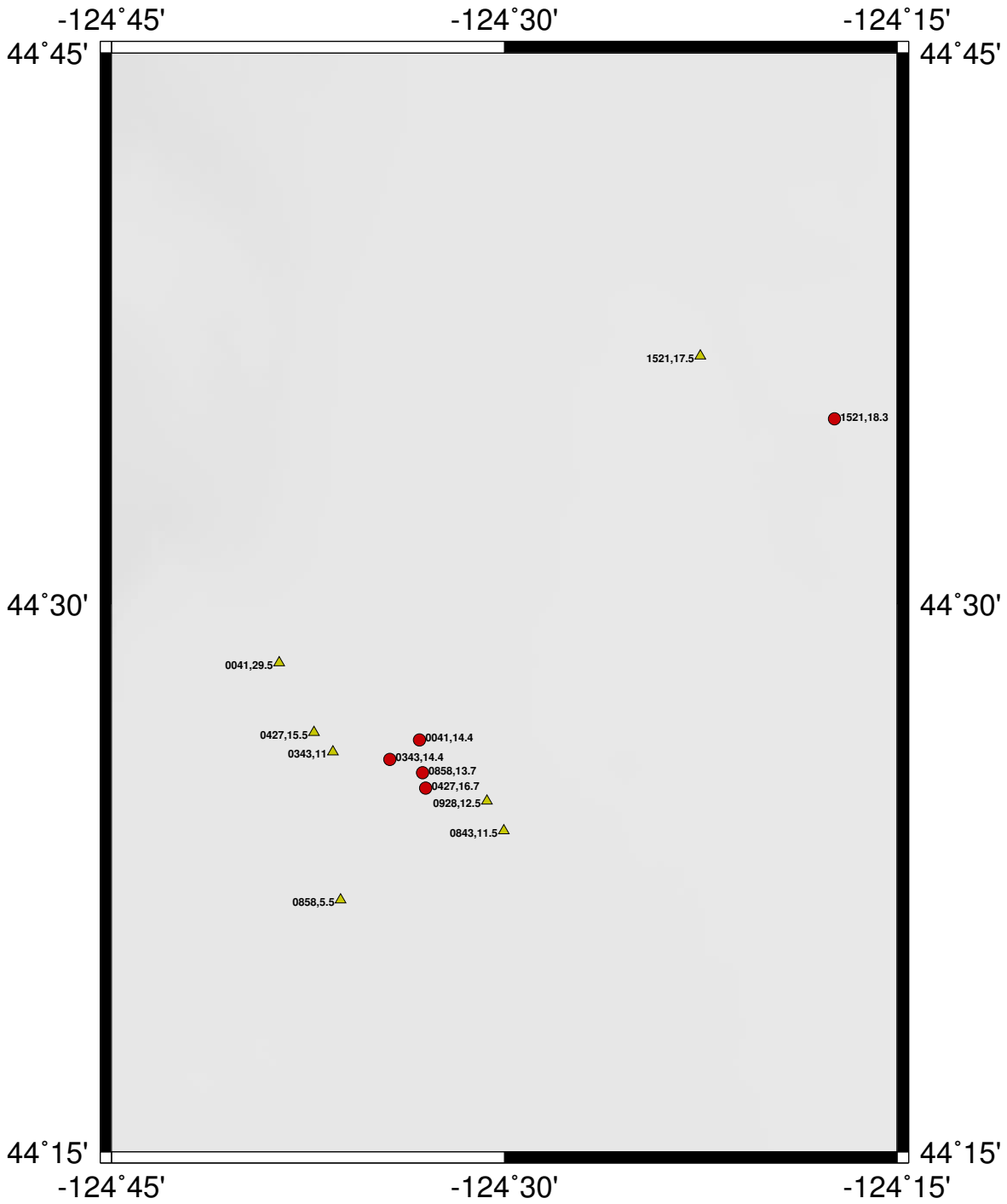

Figure 2-15: Yellow triangles shows the result of grid-search algorithm, using P arrivals with full weight to stations closer than 40 km and removing the arrivals from stations farther than 180 km combined with S arrivals using 50% weight for stations closer than 40 km. Red circles are events that located with 1D model and HYPO71 (LEE AND LAHR, 1972) algorithm (Trehu et al., 2015).

3 Discussion and Conclusion

3.1 Results and Discussion:

Figures 2-13, 2-14 and 2-15 are showing differences in hypocenter locations between hypocenter location obtained by using linearized location method HYPO71 (Lee and Lahr, 1972) and one-dimensional velocity model (Gerdom et al., 2000; Trehu et al., 2015) and relocated earthquake locations obtained from three different methods of the weighting and selecting arrival picks in this study.

There was a longitudal shift between located earthquake by Trehu et al. (2015) and our relocated events. The average shift was about 7 km toward west (Ocean) as we expected because of better station coverage on the ocean side. We could not find systematic latitudal change in the locations. Events #1 and #2 in out catalog were not located by Trehu et al., (2015) but comparing with ANSS catalog these two events shifted to the west too (about 9 km). Event #3 in our catalog happened in April 18, 2012 were relocated by Trehu et al., (2015) linearized 1D relocation method. Figures 2-13 through 2-15 and tables 2-3 through 2-5 show if we use only P arrivals with tapered weighting based on distance or combine P arrivals and S arrivals following method1 or method2 in this study, Events #3 will shift to the west and slightly northward. Even if we use their picks and put that in our 3D velocity model grid-search the results will be shifting to the west and depth is not changing dramatically between these methods.

Events #4 through #7 happened in January 25, 2013. Trehu et al., (2015) located them almost in the same spot with depths close between 13.7 and 16.7 km but our results are more scattered with overall 7 km shift to the west. Epicentral pattern is extended in 10 km in the North-South direction. Depth of earthquakes variation is between 5.5 to 29.5km. Event #4 shows 29.5 km depth with all 3 methods that we used in this study and when removed effect of farther stations in method2 it shifted to the north. Event #5 shows shift to the west and more consistent latitude location in all 3 cases and depth is 15 km. Also Event #6 shows shift to the west and consistent latitudal shift to the north but depths are changing between 15.5 and 29.5 km. Event #7 location has the same shift to South-West direction in all 3 methods of weighting and selecting arrivals and depth is almost the same and about 6km (ranges between 5.5 to 6.5km).

We looked at the residuals for all events in each method. Figures 3-1 to 3-14 are showing the residuals based on distances between events and stations and azimuth using only P arrivals tapered weighting function based on distance (Table 2-1). Different colors of scatter plots are showing different weights for arrivals in these stations.

As we can see residuals for P arrivals are very small (less than 0.5 s) for most of the close stations (less than 120 km). But still some close stations in East side of the events (located on land) are showing large residuals. Unfortunately, S residual patterns are showing unacceptable values such 3 seconds many of the stations on the east side of the events. After looking back to the generated velocity model we found that this issue should be related to underestimation of Vp/Vs ratio on continental block. We used a constant Vp/Vs ratio of 1.8 on continental and oceanic crust part of the velocity model to generating S wave travel times. Vp/Vs ratio on continental crust is about 2 and it means our model have underestimation of Vs value and that's the reason of we getting large negative residuals in stations on east side of the cluster.

3.2 Conclusion:

We used probabilistic, nonlinear earthquake location to relocate the earthquakes on Cascadia continental margin. The NonLinLon program allows us to use pseudo-3D velocity model and nonlinear solution which makes it superior to traditional, linearized solutions methods.

Our earthquake relocation results in overall shift of 7 km to the west in seismicity pattern. Based on depth results 1 out of 7 events occurred in overriding plate. 5 events seem be occurred on plate interface and one event depth is located in the base of oceanic crust. Plate interface in our model is located in about 15 km depth. But in order to get better understanding of seismicity and including more reliable S arrivals in our analysis we have to do the correction on Vp/Vs ration on continental block and relocate all events on Continental Margin with grid-search methods that contains S arrival picks as well.

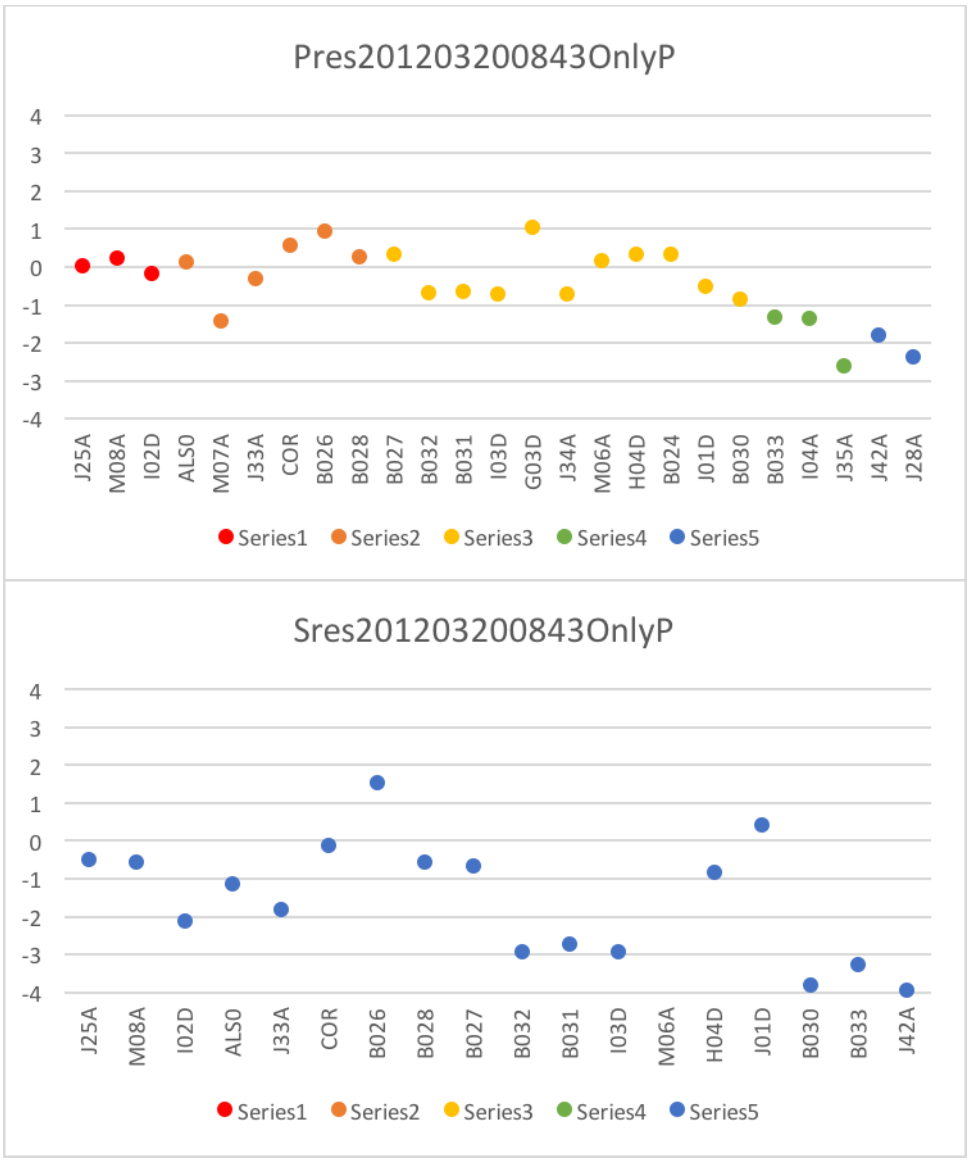

Figure 3-1: Residuals for Event#1, Only P arrival used for location.

Top: P residuals based on distance. Bottom: S residuals based on distance.

series 1, 2, 3, 4 and 5 are showing the weighting 100%, 75%, 50%, 25% and 0% respectively.

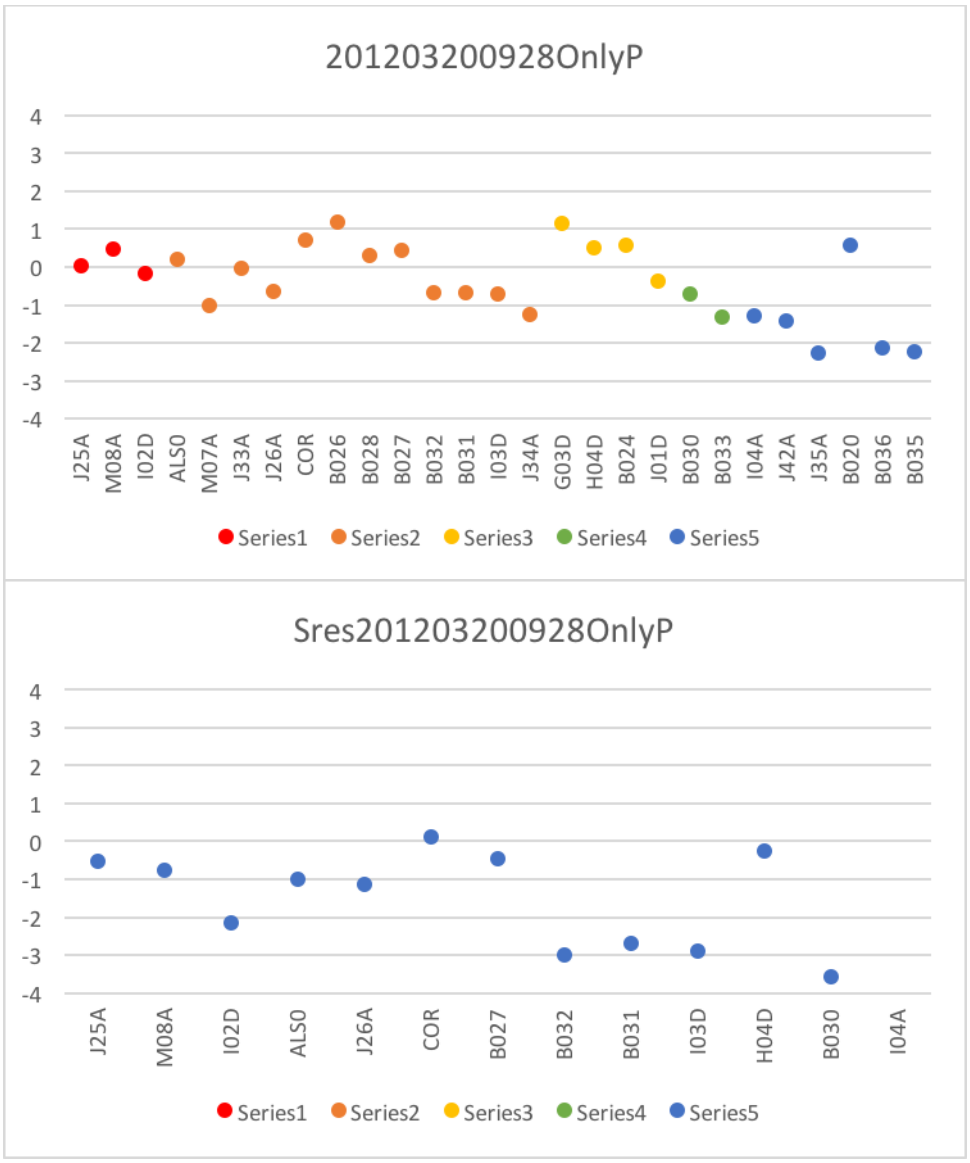

Figure 3-2: Residuals for Event#2, Only P arrival used for location.

Top: P residuals based on distance. Bottom: S residuals based on distance.

series 1, 2, 3, 4 and 5 are showing the weighting 100%, 75%, 50%, 25% and 0% respectively.

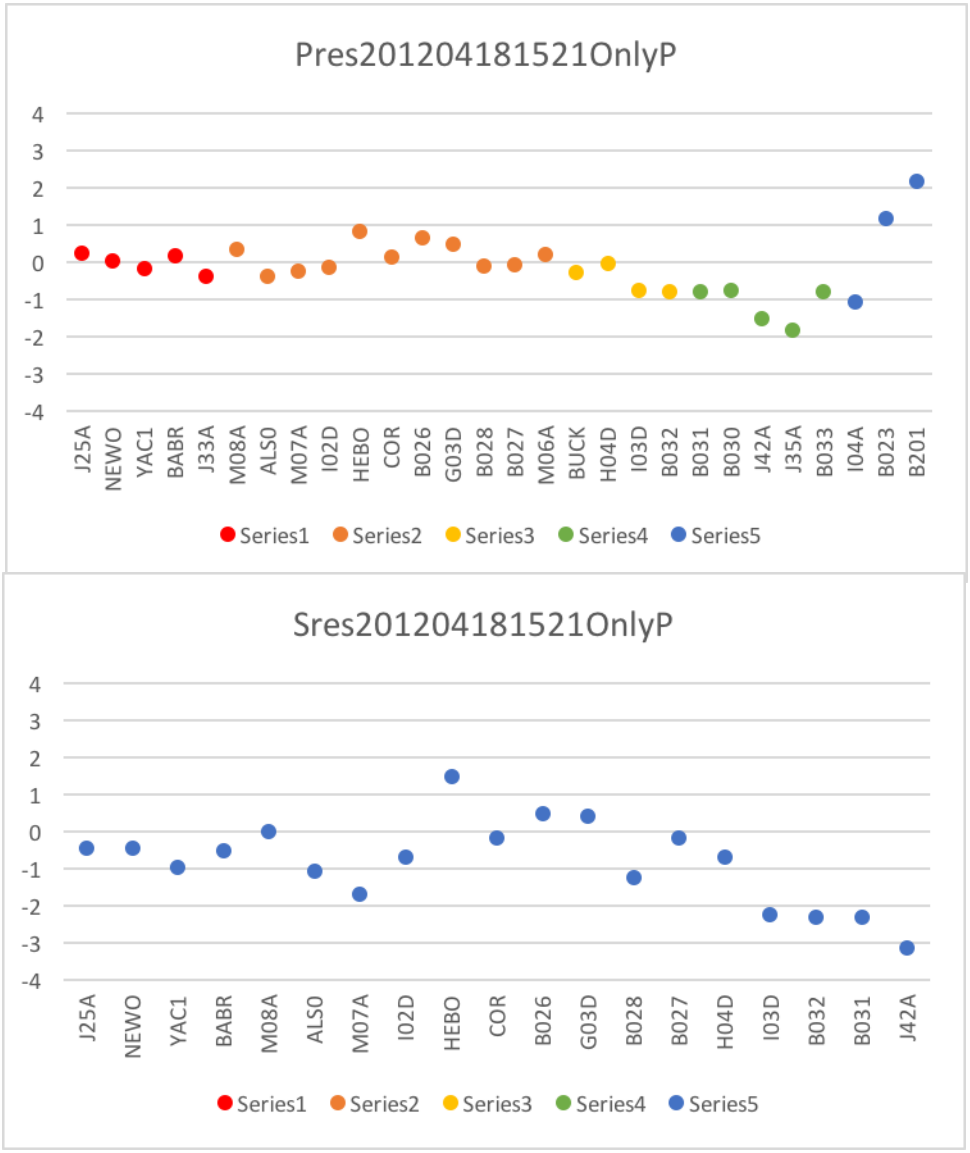

Figure 3-3: Residuals for Event#3, Only P arrival used for location.

Top: P residuals based on distance. Bottom: S residuals based on distance.

series 1, 2, 3, 4 and 5 are showing the weighting 100%, 75%, 50%, 25% and 0% respectively

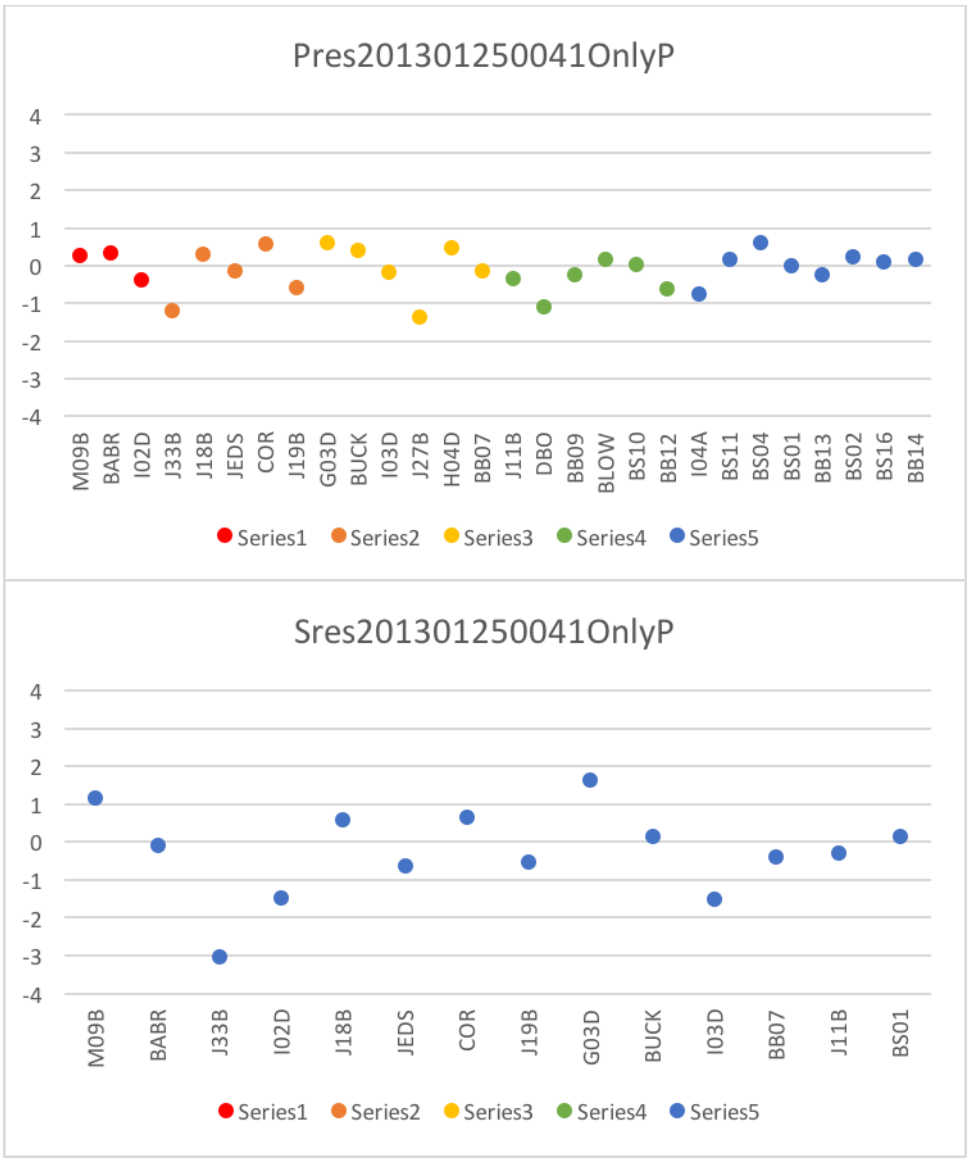

Figure 3-4: Residuals for Event#4, Only P arrival used for location.

Top: P residuals based on distance. Bottom: S residuals based on distance.

series 1, 2, 3, 4 and 5 are showing the weighting 100%, 75%, 50%, 25% and 0% respectively

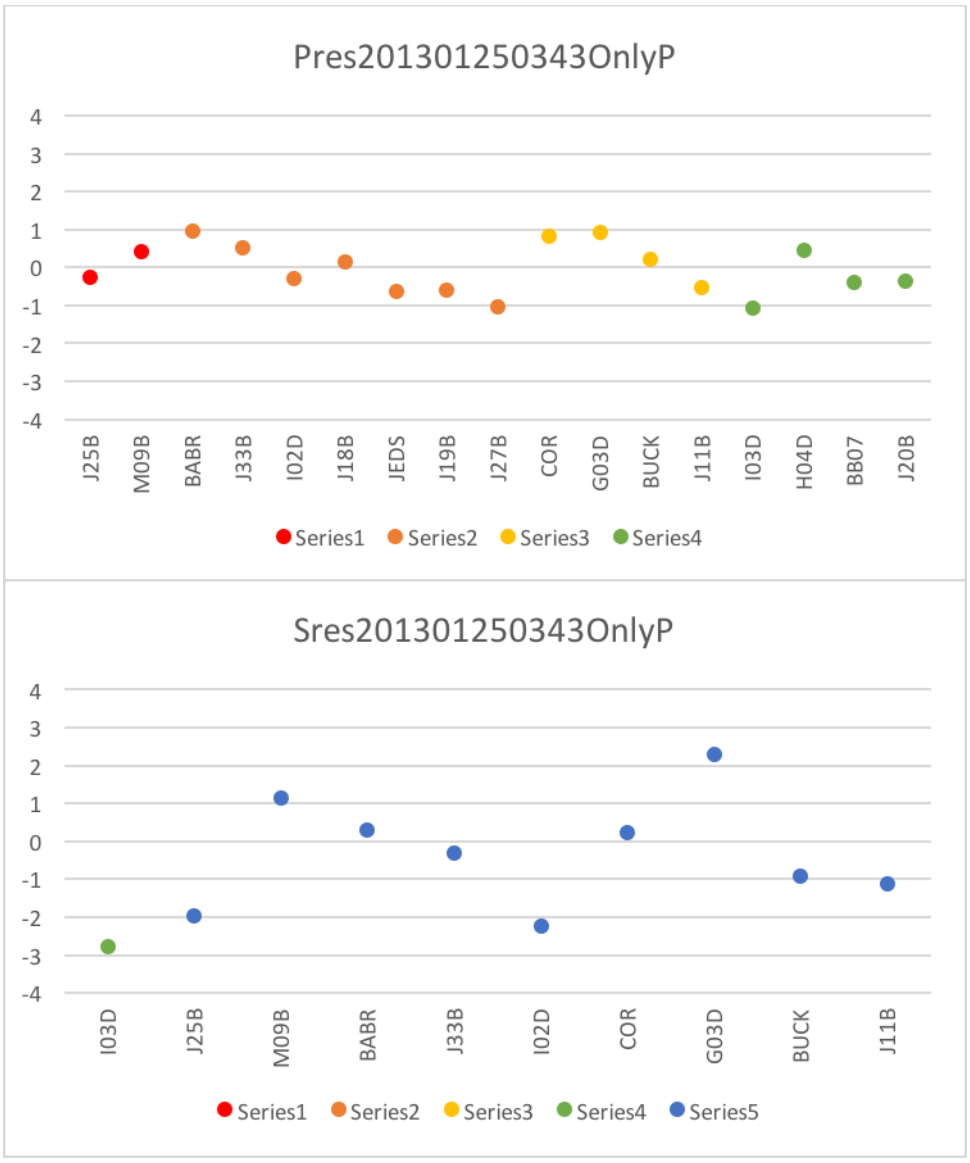

Figure 3-5: Residuals for Event#5, Only P arrival used for location.

Top: P residuals based on distance. Bottom: S residuals based on distance.

series 1, 2, 3, 4 and 5 are showing the weighting 100%, 75%, 50%, 25% and 0% respectively

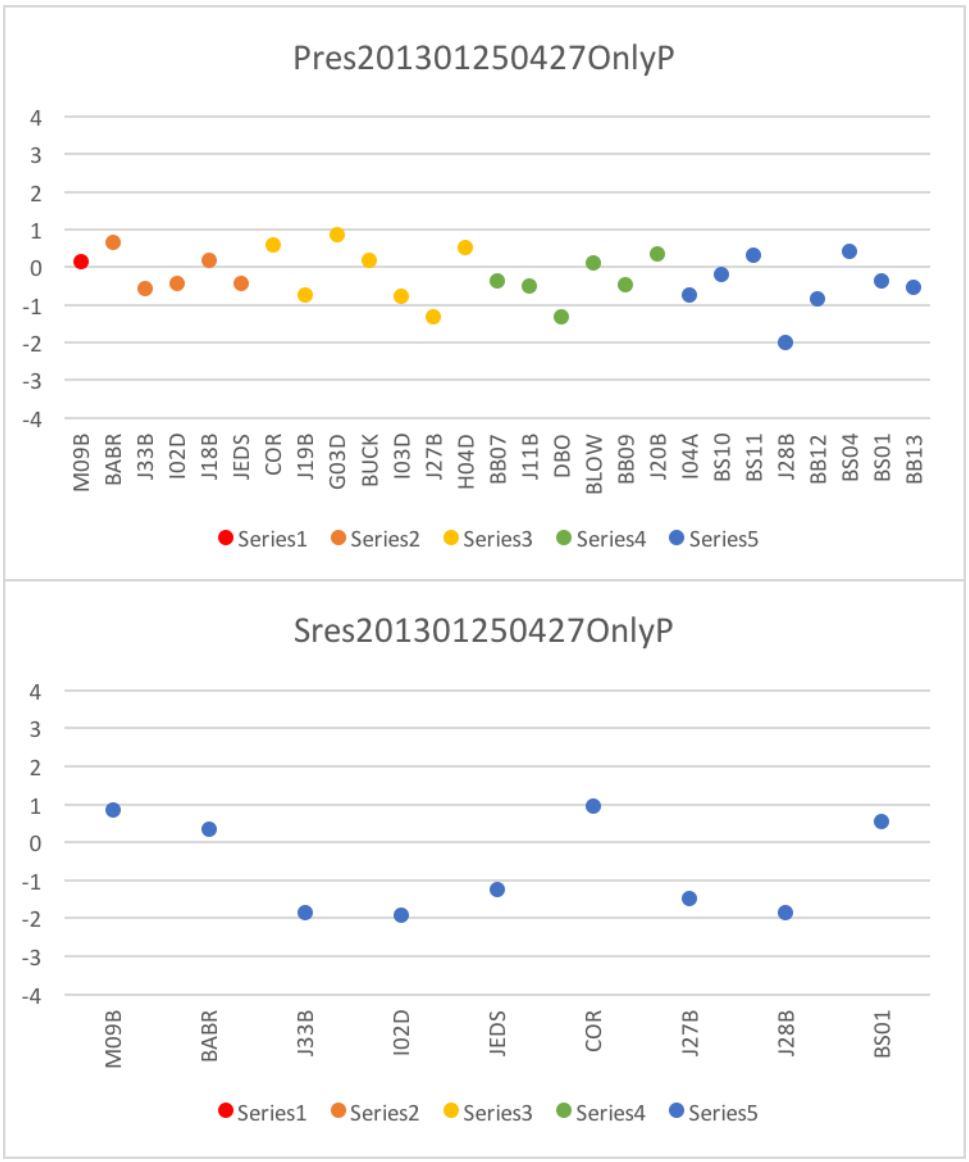

Figure 3-6: Residuals for Event#6, Only P arrival used for location.

Top: P residuals based on distance. Bottom: S residuals based on distance.

series 1, 2, 3, 4 and 5 are showing the weighting 100%, 75%, 50%, 25% and 0% respectively

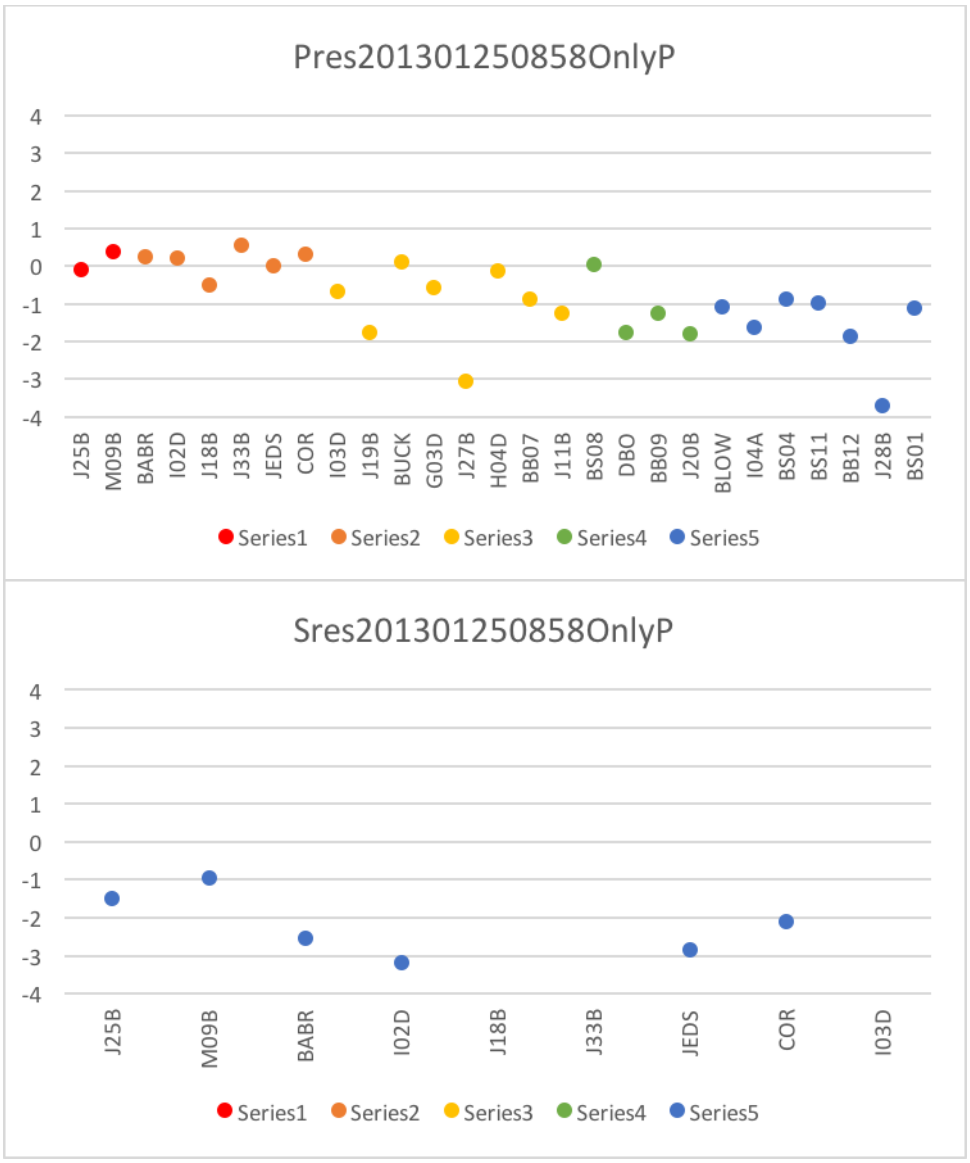

Figure 3-7: Residuals for Event#7, Only P arrival used for location.

Top: P residuals based on distance. Bottom: S residuals based on distance.

series 1, 2, 3, 4 and 5 are showing the weighting 100%, 75%, 50%, 25% and 0% respectively

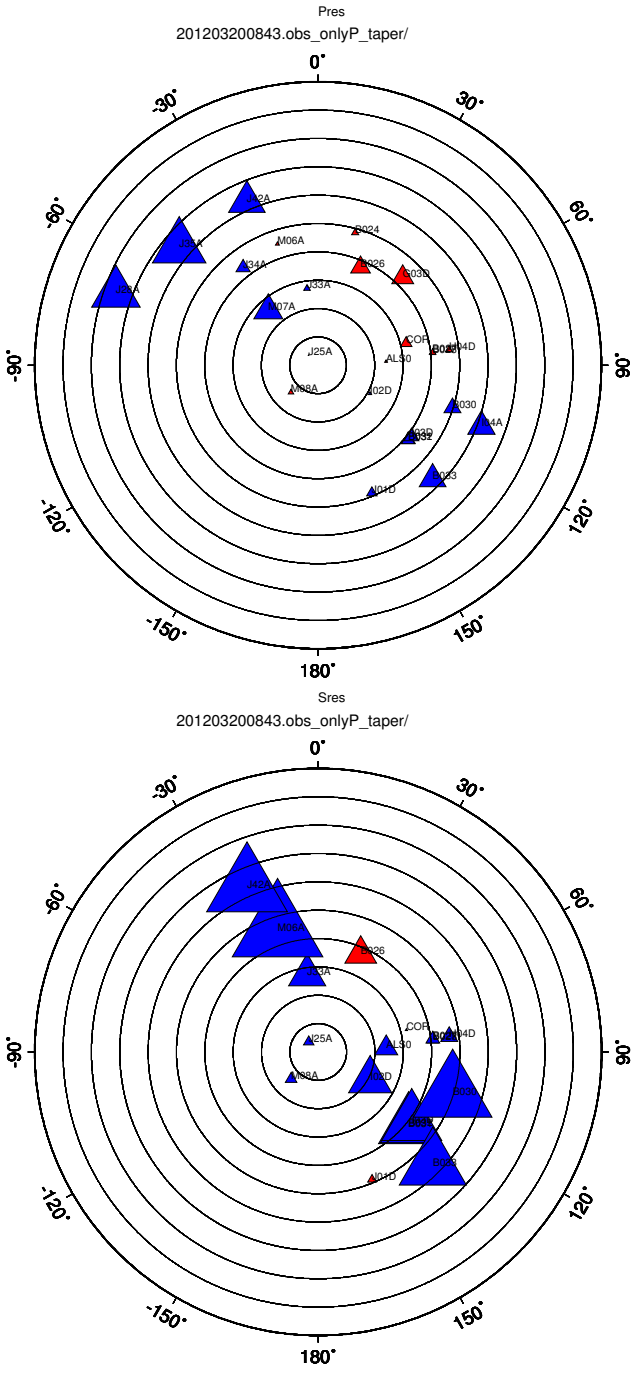

Figure 3-8: Residuals based on azimuth and distance for Event#1

Top: P residuals, Bottom: S residuals

Red triangles show the stations with positive residuals and blue triangles show the stations with negative residuals. Triangle's sizes are scaled based on residual 's values. Concentric circles are incremented 30 km.

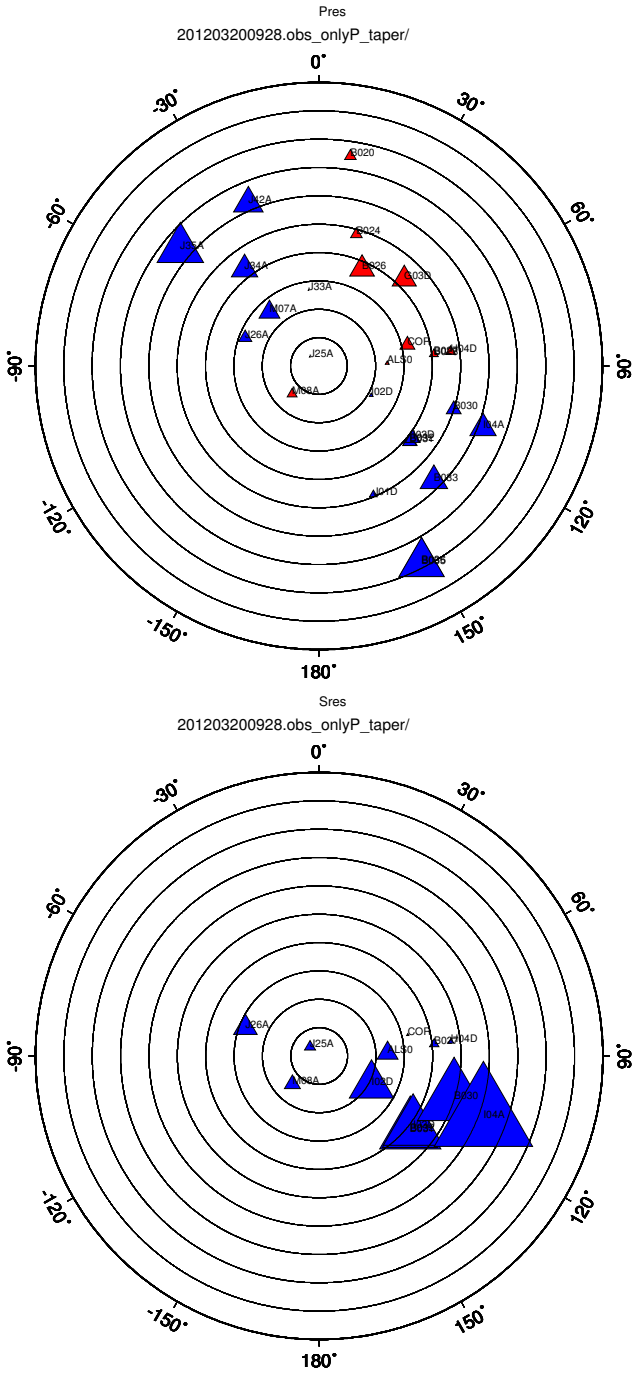

Figure 3-9: Residuals based on azimuth and distance for Event#2

Top: P residuals, Bottom: S residuals

Red triangles show the stations with positive residuals and blue triangles show the stations with negative residuals. Triangle's sizes are scaled based on residual 's values. Concentric circles are incremented 30 km.

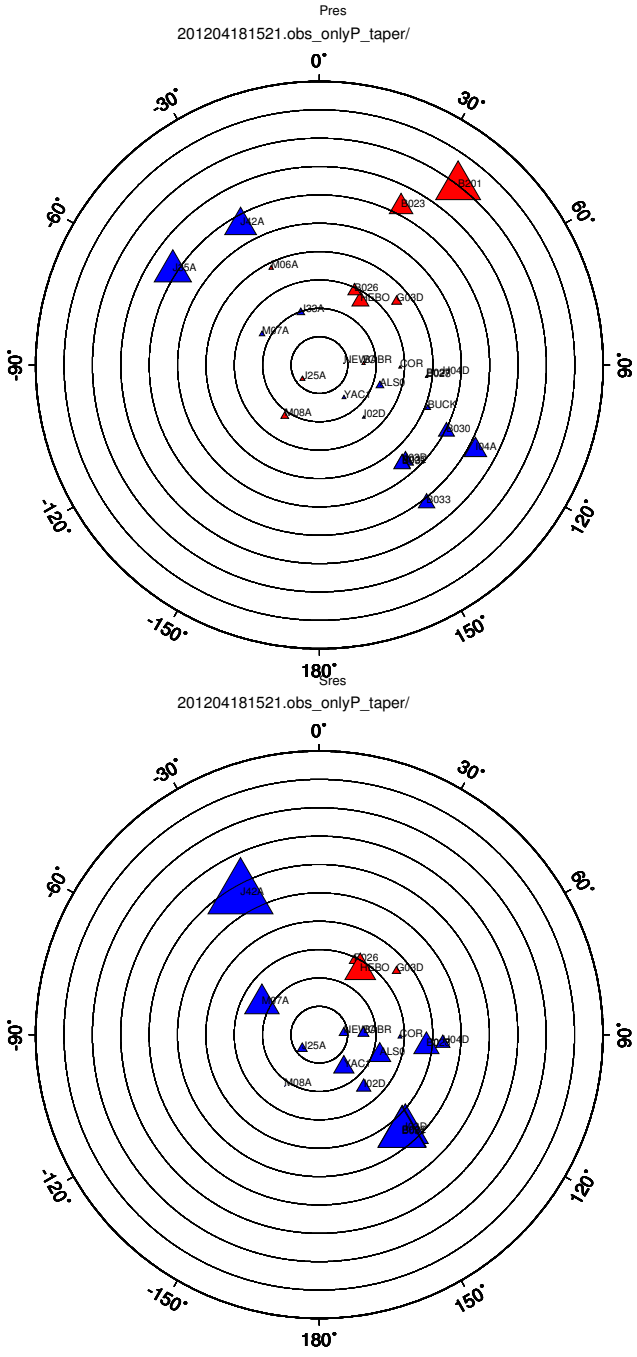

Figure 3-10: Residuals based on azimuth and distance for Event#3

Top: P residuals, Bottom: S residuals

Red triangles show the stations with positive residuals and blue triangles show the stations with negative residuals. Triangle's sizes are scaled based on residual 's values. Concentric circles are incremented 30 km.

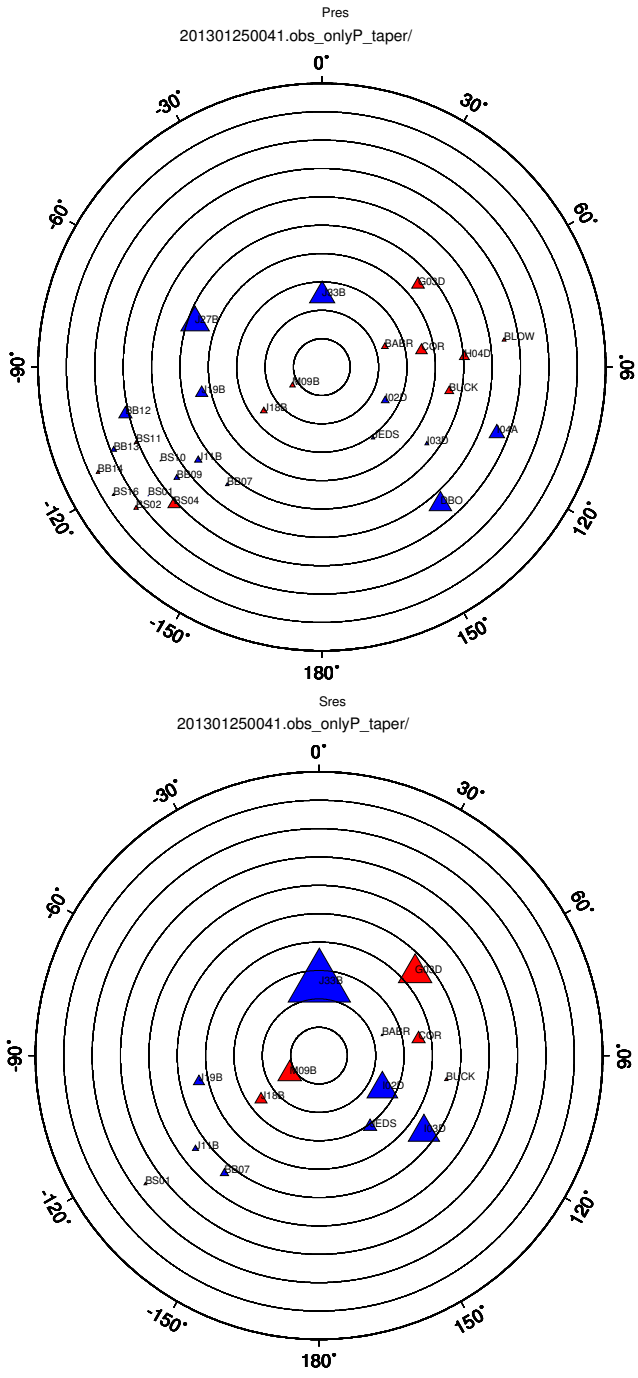

Figure 3-11: Residuals based on azimuth and distance for Event#4

Top: P residuals, Bottom: S residuals

Red triangles show the stations with positive residuals and blue triangles show the stations with negative residuals. Triangle's sizes are scaled based on residual 's values. Concentric circles are incremented 30 km.

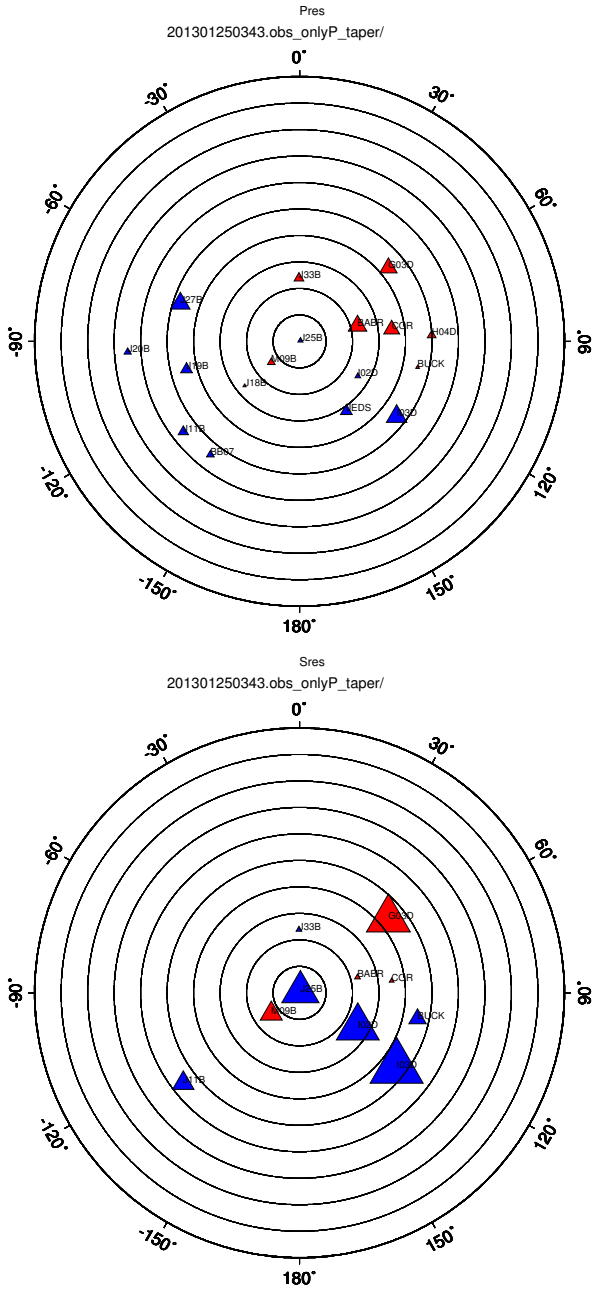

Figure 3-12: Residuals based on azimuth and distance for Event#5

Top: P residuals, Bottom: S residuals

Red triangles show the stations with positive residuals and blue triangles show the stations with negative residuals. Triangle's sizes are scaled based on residual 's values. Concentric circles are incremented 30 km.

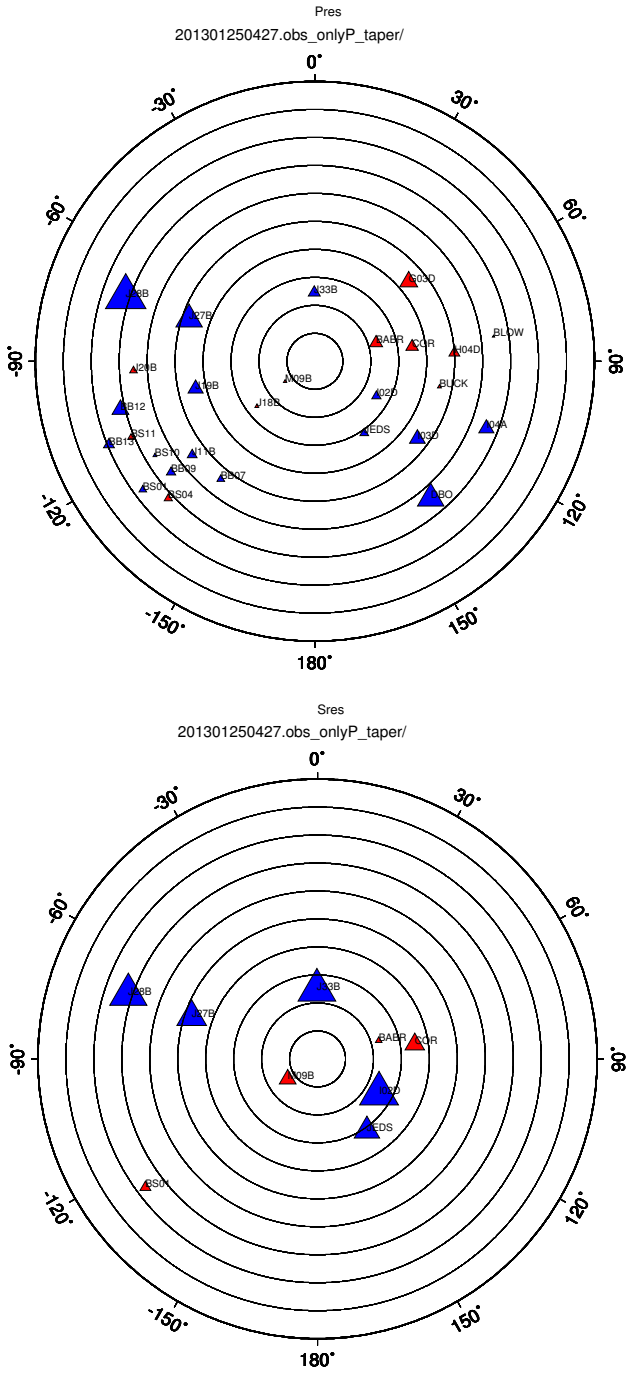

Figure 3-13: Residuals based on azimuth and distance for Event#6

Top: P residuals, Bottom: S residuals

Red triangles show the stations with positive residuals and blue triangles show the stations with negative residuals. Triangle's sizes are scaled based on residual 's values. Concentric circles are incremented 30 km.

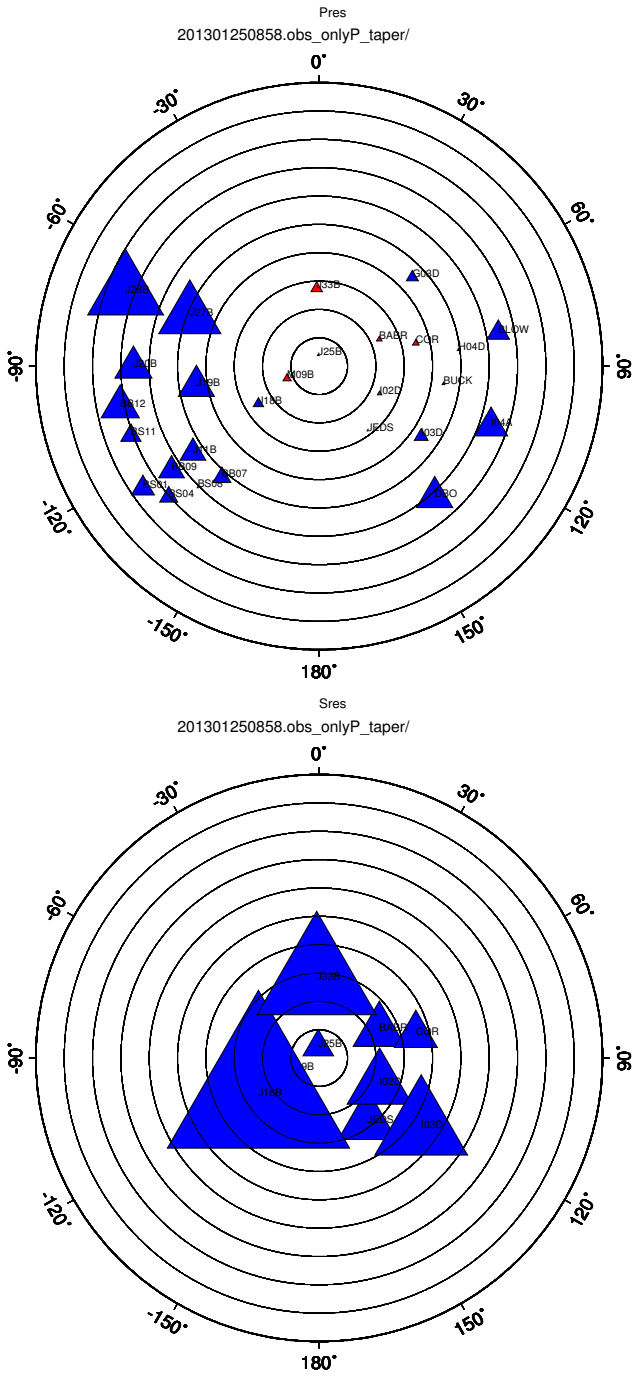

Figure 3-14: Residuals based on azimuth and distance for Event#7

Top: P residuals, Bottom: S residuals

Red triangles show the stations with positive residuals and blue triangles show the stations with negative residuals. Triangle's sizes are scaled based on residual 's values. Concentric circles are incremented 30 km.

References:

Gerdom, M., A. M. Tréhu, E. R. Flueh, and D. Klaeschen (2000). The continental margin off Oregon from seismic investigations, Tectonophysics 329, 79–97.

Goldfinger C, Nelson CH, Johnson JE. (2003). Holocene earthquake records from the Cascadia subduction zone and northern San Andreas Fault based on precise dating of offshore turbidites. Annual Review of Earth and Planetary Sciences 31, 555–577.

Goldfinger, C., C. H. Nelson, A. Morey, J. E. Johnson, J. Gutierrez- Pastor, A. T. Eriksson, E. Karabanov, J. Patton, E. Gracia, R. Enkin, A. Dallimore, G. Dunhill, and T. Vallier (2012). Turbidite event history: Methods and implications for Holocene paleoseismicity of the Cascadia Subduction Zone, U.S. Geol. Surv. Profess. Pap. 1661-F, Reston, Virginia, 332 pp., 64 Figures.

Husen, E., R.B. Smith, Probabilistic earthquake relocation in three-dimensional velocity models for the Yellowstone National Park Region Wyoming, Bull. Seismol. Soc. Am., 94 (3) (2004), pp. 880–896

Lee, W. H. K. and J. C. Lahr (1972). HYP071: A computer program for determining hypocenter, magnitude, and first motion pattern of local earthquakes, Open File Report, U. S. Geological Survey, 100 pp.

Lomax, A., J. Virieux, P. Volant, and C. Thierry-Berge (2000). Probabilistic earthquake location in 3D and layered models, in Advances in Seismic Event Location, C. H. Thurber and N. Rabinowitz (Editors), Kluwer Academic Publishers, Dordrecht/Boston/London, 101–134.

Lomax, A., and A. Curtis (2001). Fast, probabilistic earthquake location in 3D models using Oct-Tree Importance sampling. Geophys. Res. Abstr., 3.

McCaffrey, R., A. I. Qamar, R. W. King, R. Wells, G. Khazaradze, C. A. Williams, C. W. Stevens, J. J. Vollick, and P. C. Zwick (2007). Fault locking, block rotation and crustal deformation in the Pacific Northwest, Geophys. J. Int. 169, 1315–1340.

Morton, E. A., S. L. Bilek (2015). Preliminary Event Detection of Earthquakes Using the Cascadia Initiative Data, Seismological Research Letters, 2015 Sep-Oct, Vol.86(5), pp.1270-1277.

Moser, T. J., T. van Eck, and G. Nolet (1992). Hypocenter determination in strongly heterogeneous earth models using the shortest path method, J. Geophys. Res. 97, 6563–6572.

Pavlis, G. L., F. Vernon, D. Harvey, and D. Quinlan (2004). The generalized earthquake-location (GENLOC) package: An earthquake-location library, Comput. Geosci. 30, 1079-1091

Satake K, Shimazaki K, Tsuji Y, Ueda K. 1996. Time and size of a giant earthquake in Cascadia inferred from Japanese tsunami records of January 1700. Nature 379:246–49

Satake K, Atwater BF (2007) Long-term perspectives on giant earthquakes and tsunamis at subduction zones. Annual Review of Earth and Planetary Sciences 35: 349–374.

Tarantola, A., and B. Valette (1982). Inverse problems Quest for infor- mation, J. Geophys. Res. 50, 159–170.

Toomey, D. R., R. M. Allen, A. H. Barclay, S. W. Bell, P. D. Bromirski, R. L. Carlson, X. Chen, J. A. Collins, R.P. Dziak, B. Evers, et al. (2014). The Cascadia Initiative: A sea-change in seismological studies of subduction zones, Oceanography 27, 116–128.

Tréhu, A. M., R. J. Blakely, and M. C. Williams (2012). Subducted seamounts and recent earthquakes beneath the central Cascadia forearc, Geology 40, 103–106.

Tréhu, A. M., J. Braunmiller, and J. L. Nabelek (2008). Probable low- angle thrust earthquakes on the Juan de Fuca–North America plate boundary, Geology 36, 127–130.

Tréhu, A. M., J. Braunmiller, and E. Davis (2015). Seismicity of the Cascadia Continental Margin near 44.5 N: A Decadal View, Seismological Research Letters, 2015 May-June, Vol.86(3), pp.819-829.

Williams, M. C., A. M. Tréhu, and J. Braunmiller (2011). Seismicity at the Cascadia plate boundary beneath the Oregon continental shelf, Bull. Seismol. Soc. Am. 101, 940–950.